et al., 1996; Wang & Linden, 2000). For example, insulin/insulin-like growth factor-I can induce LTD in PCs (Wang & Linden, 2000). Lavendustin A and herbimycin A, inhibitors of protein-tyrosine kinases (PTKs), suppress cerebellar LTD (Boxall *et al.*, 1996). However, the roles of tyrosine phosphorylation events in cerebellar LTD and motor learning remain to be established.

PTPMEG/PTPN4 is a cytoplasmic protein-tyrosine phosphatase (PTP) containing protein 4.1 and Ezrin/Radixin/Moesin (FERM) and postsynaptic density-95/discs-large/ZO-1 (PDZ) domains, which was originally identified from a megakaryoblastic cell line (Gu *et al.*, 1991). Although overexpression of PTPMEG in COS-7 cells inhibits cell proliferation (Gu *et al.*, 1996), physiological roles of PTPMEG have not been elucidated. We previously showed that PTPMEG mRNA was expressed at high levels in PCs and the thalamus, and that PTPMEG bound to the carboxyl-terminus of GluRδ2 via the PDZ domain of PTPMEG (Hironaka *et al.*, 2000). Because GluRδ2 is essential for both cerebellar development including synapse formation and cerebellar function, such as motor coordination and motor learning (Kashiwabuchi *et al.*, 1995; Kishimoto *et al.*, 2001c; Yuzaki, 2004), PTPMEG may also play a role in the cerebellar function. In this study, we generated PTPMEG-knockout (KO) mice, and found that these mice showed impairment in memory formation of motor learning and cerebellar LTD at PF–PC synapses.

Materials and methods

Generation of PTPMEG-KO mice

P1 clones carrying PTPMEG genomic sequences were obtained from a mouse ES-129/SvJ genomic library. The targeting vector was constructed, in which a Tau-LacZ cassette (Callahan & Thomas, 1994) and a PGK-neo expression cassette were inserted at the translational initiation codon of the PTPMEG gene. The linearized vector was electroporated into E14 ES cells, and G418-resistant clones with the anticipated homologous recombination were screened by polymerase chain reaction and Southern blotting. Chimeric mice were generated by an aggregation method. Male chimeras were mated with C57BL/6J females to obtain PTPMEG heterozygous mice (F1) with a 50% pure C57BL/6J genetic background. Heterozygous mice were successively backcrossed with C57BL/6J mice. F3 heterozygous mice were crossed to each other to obtain wild-type and PTPMEG-KO littermates. All behavioral and electrophysiological analyses were done in a blind manner to genotypes. Experiments with animals were carried out in accordance with the guidelines for animal use issued by the Committees of Animal Experiments of Institute of Medical Science, University of Tokyo, Kanazawa University, and Osaka University.

Preparation of cerebellar lysates and immunoblotting

Mice aged 4 days to 30 weeks were anaesthetized with diethyl either and their cerebella were lysed in a Tris/NP-40/EDTA buffer, and the lysates were subjected to immunoblotting as described (Hironaka *et al.*, 2000). A rabbit anti-PTPMEG antibody was described previously (Hironaka *et al.*, 2000). An anti-α-tubulin monoclonal antibody and an anti-Erk1 antibody were purchased from Sigma-Aldrich (St Louis, MO, USA) and Santa Cruz Biotechnology (Santa Cruz, CA, USA), respectively.

Histology

Mice aged 8 weeks were anaesthetized with diethyl ether and perfused with 4% paraformaldehyde/phosphate-buffered saline under deep ether anesthesia. Parasagittal cerebellar sections (20 μm thickness) were prepared by use of a cryostat, and stained with Cresyl violet or immunostained with an anti-calbindin antibody (SWANT, Bellinzona, Switzerland), followed by Alexa488-labeled goat anti-mouse IgG (Invitrogen, Carlsbad, CA, USA). The immunoreactive signals were obtained by a confocal microscopy (Olympus, Tokyo, Japan).

Animal behavioral analysis

Fixed-bar test

The fixed bar consisted of wood (either 6 mm or 20 mm in width, 80 cm in length, and 40 cm above the ground) was held horizontally on both ends. A mouse aged 8–10 weeks was placed on the bar, and the time was measured for which each mouse remained on the bar for a maximum of 60 s (Kadotani *et al.*, 1996). Data were statistically analysed by *t*-test. The difference was considered significant when P was less than 0.05.

Accelerated rotarod test

A mouse aged 8–9 weeks was placed on a drum (3 cm in diameter, polyvinyl chloride: Ohara, Tokyo, Japan) rotating at 4 r.p.m. at the beginning and, then, the rotation of the rotarod was accelerated from 4 to 40 r.p.m. over a 300-s period at a constant rate (Miyakawa *et al.*, 2001). The time was measured for which each mouse was able to maintain its balance on the rod. Mice were trained for two consecutive days, receiving four trials per day at intervals of 2 h between trials. Data were statistically analysed by a two-way repeated measures ANOVA. A *post hoc* comparison between the two genotypic groups for each trial was made with *t*-test (Granon *et al.*, 2003). The difference was considered significant when P was less than 0.05.

Classical eyeblink conditioning

Mice underwent surgery at the age of 8–11 weeks and conditioning experiments started at the age of 9–12 weeks. The surgical and conditioning procedures were basically the same as described previously (Kishimoto *et al.*, 2001c). Mice were anesthetized with ketamine (80 mg/kg, i.p.; Sankyo, Tokyo, Japan) and xylazine (20 mg/kg, i.p. Bayer, Tokyo, Japan). Four Teflon-coated stainless-steel wires (100 μm in diameter, A-M Systems, WA, USA) were implanted subcutaneously under the left eyelid. The two wires were used to record electromyograms (EMG) in the orbicularis oculi muscle that detects an eyeblink, and the remaining two to deliver electrical shocks [unconditioned stimulus (US)]. A 100-ms periorbital shock (100 Hz square pulses) was used as the US, and a 450-ms tone (1.0 kHz, 80 dB) was used as the conditioned stimulus (CS). The US intensity was carefully determined as the minimal current amplitude required for eliciting an eyeblink response (about 0.2–0.3 mA) and constant unconditioned response (UR) amplitude (maximum EMG amplitude = 400%). In the delay eyeblink conditioning, the US overlapped the CS in time such that the two stimuli terminate simultaneously. The acquisition session consisted of 10 CS-only (every 10th trial) and 90 CS–US paired trials. The extinction session consisted of 100 CS-only trials. In pseudo-conditioning, the CS and US were randomly presented at an interstimulus interval ranging from 0 to 20 s. The spontaneous eyeblink frequency was measured by 100 'no stimulus' trials before the conditioning experiment began, and the startle response to a tone was measured during the initial 100 trials of the first session of the delay eyeblink conditioning. The UR amplitude was defined as the EMG amplitude at 50 ms after the US onset. All

experiments were performed during the light phase of a light : dark cycle in a container (10 cm in diameter) placed in a sound- and light-attenuating chamber. Data were statistically analysed by a two-way repeated measures ANOVA. A *post hoc* comparison between the two genotypic groups on each day was made with *t*-test. The difference was considered significant when P was less than 0.05 (Kishimoto *et al.*, 2001c, 2002; Granon *et al.*, 2003).

Electrophysiology

In the experiments in which the innervation patterns of CFs, the responses to paired pulses and the amplitude–intensity curve of the PF–PC synapses were examined, parasagittal cerebellar slices (250 μm thickness) were prepared from mice aged 4–9 weeks as described (Kano *et al.*, 1995; Kurihara *et al.*, 1997; Hashimoto *et al.*, 2001). The animals were anaesthetized with CO_2, and whole-cell recordings were made from visually identified PCs using an upright microscope (Olympus BX51WI) at 31 °C. Resistances of patch pipettes were 3–6 MΩ when filled with an intracellular solution composed of (in mM): CsCl, 60; Cs D-gluconate, 10; TEA-Cl, 20; BAPTA, 20; $MgCl_2$, 4; ATP, 4; GTP, 0.4; HEPES, 30 (pH 7.3). The pipette access resistance was compensated by 70–80%. The composition of standard bathing solution was (in mM): NaCl, 125; KCl, 2.5; $CaCl_2$, 2; $MgSO_4$, 1; NaH_2PO_4, 1.25; $NaHCO_3$, 26; glucose, 20; bubbled continuously with a mixture of 95% O_2 and 5% CO_2 (Hashimoto *et al.*, 2001). Bicuculline (10 μM) was always added to block inhibitory synaptic transmission mediated by γ-aminobutyric acid $(GABA)_A$ receptors. Excitatory postsynaptic currents (EPSCs) were recorded with an Axopatch 1D amplifier (Axon Instruments, Union City, CA, USA). The signals were filtered at 2 kHz and digitized at 20 kHz. On-line data acquisition and off-line data analysis were performed using PULSE software (HEKA, Lambrecht, Pfalz, Germany). Stimulation pipettes (5–10 μm in tip diameter) were filled with the standard saline and used to apply square pulses for focal stimulation (duration, 0.1 ms; amplitude, 0–90 V). CFs were stimulated in the granule cell layer 50–100 μm away from the PC soma. PFs were stimulated in the molecular layer.

In the experiments in which cerebellar LTD was examined, parasagittal cerebellar slices (250 μm thickness) were prepared from mice aged 8 weeks (anaesthetized with diethyl ether) and recorded basically as described (Namiki *et al.*, 2005; Kakizawa *et al.*, 2007). Resistances of patch pipettes were 1.8–3 MΩ when filled with an intracellular solution composed of (in mM): CsCl, 60; Cs D-gluconate, 40; TEA-Cl, 20; EGTA, 1; $MgCl_2$, 4; ATP, 4; GTP, 0.4; HEPES, 30 (pH 7.3). To monitor the amplitude of PF-mediated EPSCs (PF-EPSCs), test pulses were applied to PFs at 0.1 Hz, except for the period of conjunctive stimulation. The membrane potentials were held at −90 to −80 mV, after the compensation of liquid junction potential. The intensity of the stimulus was adjusted to evoke PF-EPSCs whose initial amplitudes were within the range between 100 and 200 pA. After the stable initial recording for at least 10 min, LTD was induced by the conjunctive stimulus, which was composed of 300 single PF stimuli in conjunction with a depolarizing pulse (for 50 ms from a holding potential of −90 or −80 mV to 0 mV) repeated at 1 Hz (Fujiwara *et al.*, 2007). The amplitude of PF-EPSC was normalized to the mean initial value recorded for 10 min before the conjunctive stimulus. Series resistance and membrane resistance were monitored throughout the experiments, and the data were discarded when either of these parameters changed by more than 10%. The data were also discarded when the slope of the baseline of PF-EPSC amplitudes during the initial recording for 10 min was larger than 2% (> 0.2% per min) or when the amplitude did not become stable within 30 min after the onset of whole-cell configuration (Namiki *et al.*, 2005; Kakizawa *et al.*, 2007).

Results

Generation of PTPMEG-KO mice

A targeting vector was constructed with a Tau-LacZ cassette inserted into the initiation codon of the PTPMEG open-reading frame (Fig. 1A). Targeted embryonic stem cells were selected, and correct integration of the targeting vector was confirmed by Southern blotting with PTPMEG- (Fig. 1B) and neomycin-resistance gene-specific probes (data not shown). The absence of PTPMEG expression was verified by Northern analysis (data not shown) and immunoblotting (Fig. 1C). The amount of PTPMEG in cerebellar lysates increased during postnatal development and peaked at 3–4 weeks after birth (Fig. 1D). Mice of all three genotypes were obtained at the expected Mendelian frequencies. PTPMEG-KO mice were fertile, and could be maintained for at least 16 months. Because we found defects of cerebellar functions in PTPMEG-KO mice (see below), we carried out histological examination of the cerebellum. In Nissl-stained sections, the main lobulation, the trilaminar organization of the cerebellar cortex and the monolayer alignment of PCs were grossly maintained in PTPMEG-KO mice (Fig. 1E and F). In addition, the immunohistochemical analysis for calbindin, a marker protein of PCs, did not reveal obvious defects in the development of PCs in PTPMEG-KO mice (Fig. 1G). Therefore, although subtle alterations could not be excluded, the normal cerebellar development was grossly maintained in PTPMEG-KO mice.

Impaired performance of PTPMEG-KO mice in the accelerated rotarod test

To evaluate the ability of motor coordination, we first performed the fixed-bar test (Fig. 2A). Wild-type and PTPMEG-KO mice could walk smoothly and stay on the bar (20 mm in width) with no difference in the time for which the mice stayed on the bar (wild-type, 59.29 ± 0.71 s, $n = 7$; PTPMEG-KO, 59.63 ± 0.12 s, $n = 8$; mean ± SEM, $P = 0.6159$). Even when a narrower bar (6 mm in width) was used, there was no significant difference between wild-type and PTPMEG-KO mice (wild-type, 52.14 ± 4.34 s, $n = 7$; PTPMEG-KO, 49.25 ± 3.65 s, $n = 8$; mean ± SEM, $P = 0.6695$). To further evaluate motor coordination and learning of PTPMEG-KO mice, we used the accelerated rotarod test (Fig. 2B). Wild-type and PTPMEG-KO mice performed similarly on the first trial (wild-type, 44.72 ± 9.56 s, $n = 18$; PTPMEG-KO, 30.11 ± 4.81 s, $n = 18$; mean ± SEM, $P = 0.1811$), which is a parameter of motor coordination. These results, together with those of the fixed-bar test, suggest that motor coordination is normal in PTPMEG-KO mice, although subtle defects that might be found in a more difficult test could not be ruled out. During the subsequent training, the performance of PTPMEG-KO mice to balance on the rod was significantly poorer than that of wild-type mice (genotype: $F_{1,34} = 15.57$, $P = 0.0037$; trial and genotype interaction: $F_{7,238} = 2.995$, $P = 0.005$). These data suggest that PTPMEG is required for the learning of motor skills (Nolan *et al.*, 2003).

Impaired memory formation in the cerebellum-dependent delay eyeblink conditioning in PTPMEG-KO mice

Next, we asked whether PTPMEG is involved in the delay eyeblink conditioning, which is one of the most extensively studied forms of cerebellum-dependent motor learning (Thompson & Kim, 1996; Thompson *et al.*, 1997). It has been shown that the delay eyeblink conditioning, in which the CS and US are given co-terminously to

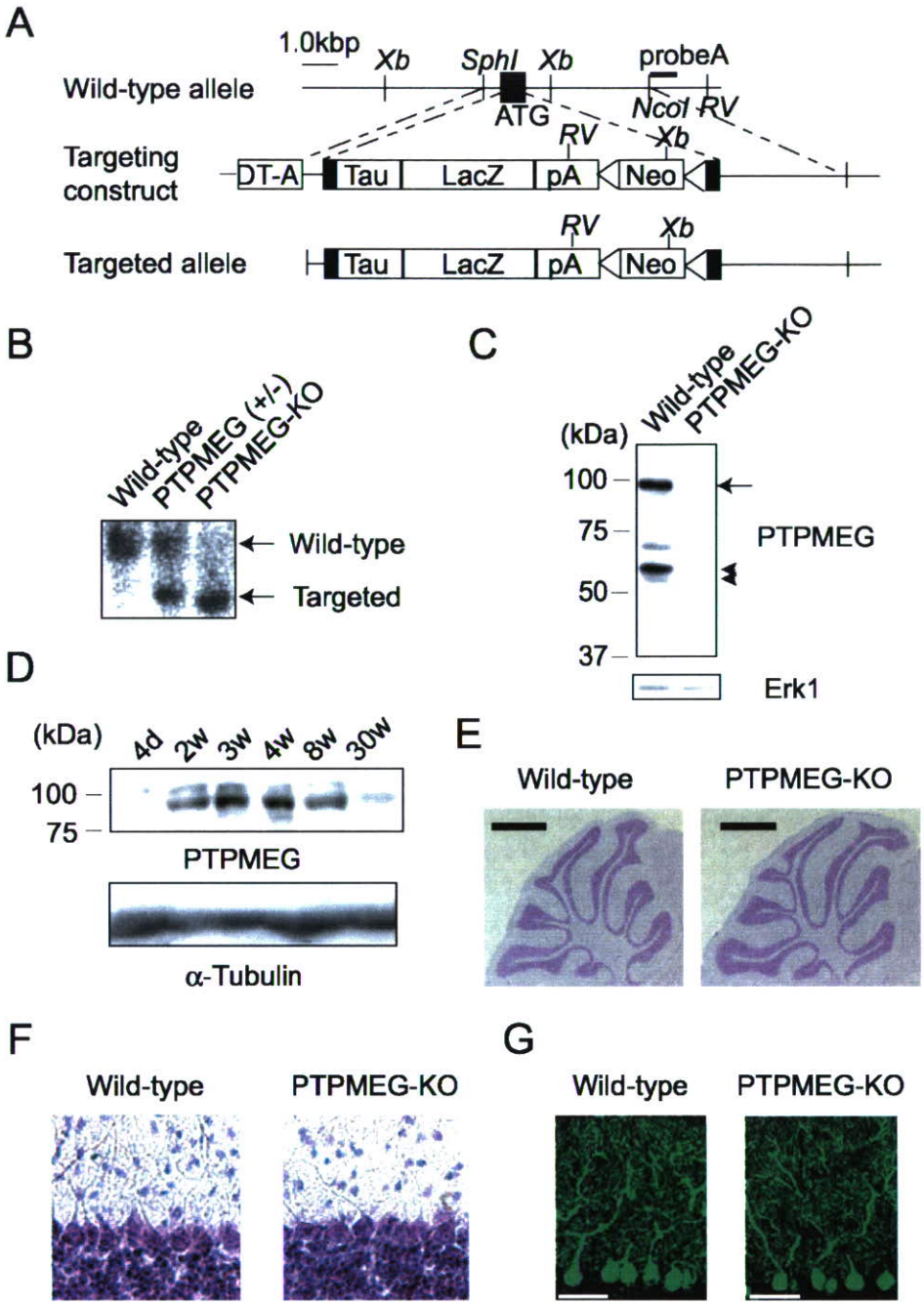

FIG. 1. Generation of PTPMEG-KO mice. (A) The restriction map of the PTPMEG genomic locus (top), targeting vector (middle) and targeted locus after homologous recombination (bottom). RV, EcoRV; Xb, XbaI. (B) Southern blot analysis. EcoRV-digested mouse tail DNAs were hybridized with probe A. A 20-kbp band and a 10.4-kbp band corresponding to wild-type and targeted alleles, respectively, were confirmed. (C) Western blot analysis. Cerebella of 8-week-old mice were lysed in a buffer containing NP-40, and the lysates were blotted with anti-PTPMEG (top) and anti-Erk1 (bottom) antibodies. The full-length (arrow) and truncated (arrowheads) products of PTPMEG are indicated, which are missing in the lysates of PTPMEG-knockout (KO) mice. (D) A temporal expression profile of PTPMEG. Cerebellar lysates from wild-type mice of the indicated ages were blotted with an anti-PTPMEG antibody (top) and an anti-α-tubulin monoclonal antibody (bottom) as a loading control. 4d, postnatal day 4; 2–30w, postnatal weeks 2–30. (E) Nissl-staining of parasagittal cerebellar sections from wild-type (left) and PTPMEG-KO (right) mice. Scale bar: 1 mm. (F) Magnified views of Nissl-stained sections. (G) Anti-calbindin immunostaining of parasagittal cerebellar sections. Scale bar: 50 μm.

mice, is cerebellum dependent (McCormick & Thompson, 1984; Chen *et al.*, 1996; Thompson *et al.*, 1997). In this paradigm, a 100-ms periorbital shock was used as the US and a 450-ms tone was used as the CS (Fig. 3B upper inset). Wild-type mice acquired the conditioned response (CR) more rapidly than PTPMEG-KO mice (Fig. 3A top). There was a significant difference between these genotypic groups (genotype: $F_{1,36} = 2.95$, $P = 0.49$; session and genotype interaction: $F_{6,216} = 4.46$, $P = 0.00028$). The deficit of CR acquisition at the early stage was more evident when analysing every 10-trial block of the daily acquisition session (Fig. 3A bottom). The sustained level of CR percentage (CR%) on Day 7 was similar between the two genotypic groups (Fig. 3A top). Consistently, the

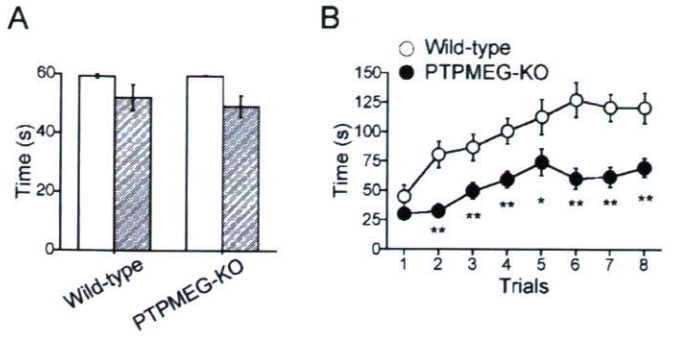

FIG. 2. Impaired performance of PTPMEG-knockout (KO) mice in the accelerated rotarod test. (A) Fixed-bar test. The time for which each mouse remained on the bar of either 20 mm (open columns) or 6 mm (hatched columns) in width was measured for a maximum of 60 s (wild-type, $n = 7$; PTPMEG-KO, $n = 8$). The data are expressed as the mean ± SEM. (B) Accelerated rotarod test. The rotation of the rod was accelerated from 4 to 40 r.p.m. over a 300-s period. A maximum retention time of 300 s was allowed for each mouse per trial. Wild-type mice (open circles, $n = 18$); PTPMEG-KO mice (closed circles, $n = 18$). The data are expressed as the mean ± SEM. $*P < 0.05$, $**P < 0.01$ (t-test).

averaged EMG amplitude for PTPMEG-KO mice was lower than that for the wild-type on Day 3, but not on Day 7 (Fig. 3B). As for the extinction of the learning, PTPMEG-KO mice showed no significant impairment at the whole extinction phase (Fig. 3A top; genotype: $F_{1,33} = 1.32$, $P = 0.26$; session and genotype interaction: $F_{3,99} = 1.53$, $P = 0.21$). These results demonstrated that PTPMEG was critical for rapid memory formation in the delay eyeblink conditioning.

No sensory deficit and the normal non-associative conditioning in PTPMEG-KO mice

There was no significant difference between wild-type and PTPMEG-KO mice in the UR amplitude in the delay eyeblink conditioning (Fig. 4A; genotype: $F_{1,33} = 0.15$, $P = 0.71$; session and genotype interaction: $F_{6,198} = 0.031$, $P = 0.99$). Furthermore, a startle response to the tone was comparable (wild-type, 2.09 ± 0.46%; PTPMEG-KO, 2.51 ± 0.53%, mean ± SEM). Next, to check a non-associative learning component, we tested the pseudo-conditioning with pseudo-randomized presentations of the CS and US (Fig. 4B). There was no significant difference between the two genotypic groups (genotype: $F_{1,8} = 0.004$, $P = 0.949$; session and genotype interaction: $F_{6,48} = 0.547$, $P = 0.769$). These results indicate that sensitivity to the CS and US, and performance of the eyeblink reflex are intact in PTPMEG-KO mice. Therefore, we concluded that the observed defects in motor learning were not likely due to deficits in the sensory perception or responses to the sensory stimuli.

Normal excitatory synaptic transmission in PCs of PTPMEG-KO mice

To investigate the abnormalities in cerebellar synaptic properties of PTPMEG-KO mice, we conducted whole-cell recordings of visually identified PCs in cerebellar slices and recorded EPSCs by stimulating CFs and PFs. We first tested whether multiple CF innervation persisted in PTPMEG-KO mice. Individual PCs are innervated by multiple CFs during early postnatal development, but supernumerary CFs are subsequently pruned, and most PCs are innervated by a single CF by 3 weeks after birth (Hashimoto & Kano, 2005). Several strains of mice with abnormal retention of multiple CF

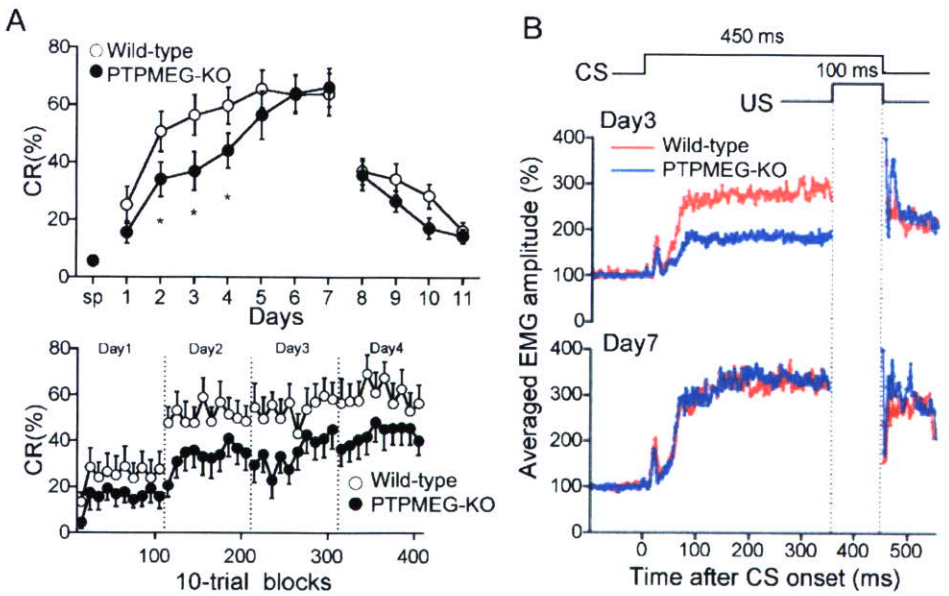

FIG. 3. Impaired acquisition of the delay eyeblink conditioning in PTPMEG-knockout (KO) mice. (A) Development of the conditioned response (CR)% during the delay eyeblink conditioning in wild-type (open circles, $n = 16$) and PTPMEG-KO (closed circles, $n = 22$) mice. (top) The averaged CR% on each day is plotted at the acquisition phase from Day 1 to Day 7. Daily sessions consisted of 10 blocks of trials. Each block consisted of nine conditioned stimulus (CS)–unconditioned stimulus (US) paired trials and one CS-only trial. At the following 4-day extinction phase, 100 CS-only presentations were given daily. 'sp' represents spontaneous eyeblink responses. The data are expressed as the mean ± SEM. $*P < 0.05$ (t-test). (bottom) When the CR% was plotted by 10-trial blocks, retarded acquisition of the CR in PTPMEG-KO mice was more clearly observed. The data are expressed as the mean ± SEM. (B) The averaged electromyogram (EMG) amplitudes of eyeblink responses for wild-type (red trace) and PTPMEG-KO (blue trace) mice on Day 3 (top) and Day 7 (bottom). Although PTPMEG-KO mice caught up with wild-type mice at the end of the training session (bottom), the top panel clearly indicates that PTPMEG-KO mice exhibited a significantly lower EMG response to the tone CS at the early stage of the conditioning training.

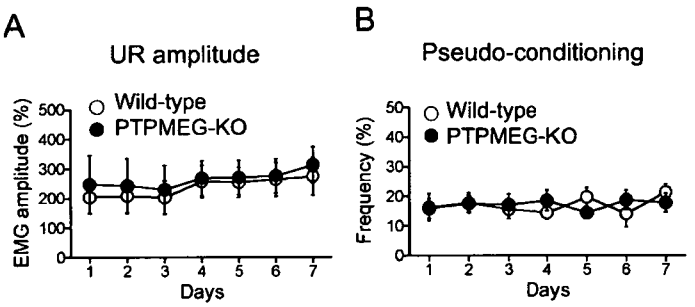

FIG. 4. Normal sensitivity to sensory stimuli and intact pseudo-conditioning in PTPMEG-knockout (KO) mice. (A) The averaged unconditioned response (UR) amplitudes for wild-type ($n = 16$) and PTPMEG-KO ($n = 22$) mice during the delay eyeblink conditioning (Fig. 3). In both genotypic groups, the UR amplitudes were nearly constant throughout the 7-day acquisition phase. No difference was observed between wild-type and PTPMEG-KO mice. (B) The pseudo-conditioning in wild-type ($n = 7$) and PTPMEG-KO ($n = 7$) mice. The CS and US were randomly presented at an interstimulus interval ranging from 0 to 20 s (10 s average). The eyelid response to the CS did not increase in either wild-type or PTPMEG-KO mice. The data are expressed as the mean ± SEM. EMG, electromyogram.

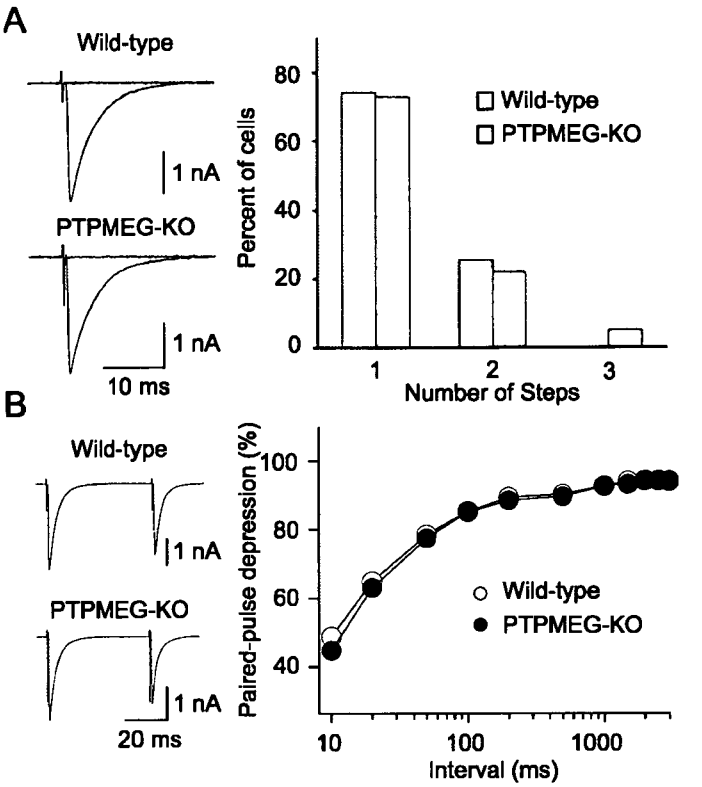

FIG. 5. Normal excitatory synaptic transmission in the CF–PC synapses of PTPMEG-knockout (KO) mice. (A) Innervation patterns of CFs. (left) Representative traces of CF-EPSCs recorded from wild-type (top) and PTPMEG-KO (bottom) PCs. CFs were stimulated in the granule cell layer at 0.2 Hz. Four traces evoked with the threshold stimulus intensity are superimposed. The holding potential was −20 mV. (right) Summary histograms showing the number of discrete steps in CF-EPSCs of wild-type (open columns, $n = 39$) and PTPMEG-KO (hatched columns, $n = 59$) PCs. The percentage of PCs with more than one discrete CF-EPSC step was similar between the two genotypic groups ($P = 0.943$, χ^2 test for independent samples). (B) Short-term synaptic plasticity of CF-EPSCs. (left) Representative traces of CF-EPSCs evoked by paired pulses at an interpulse interval of 50 ms. Three traces were averaged. (right) Summary graph showing paired-pulse depression of CF-EPSCs in wild-type (open circles, $n = 11$) and PTPMEG-KO (closed circles, $n = 14$) PCs. The amplitude of the second response is expressed as a percentage of the first response (mean ± SEM) and is plotted as a function of interpulse intervals. Stimulus pairs were applied at 0.2 Hz. The holding potential was −20 mV.

innervation, such as PKCγ- and GluRδ2-KO mice, show impaired motor coordination (Kano *et al.*, 1995; Hashimoto *et al.*, 2001). As shown in Fig. 5A, the distribution of PCs in terms of the number of CF-mediated EPSC (CF-EPSC) steps was not significantly different between wild-type and PTPMEG-KO mice ($P = 0.943$, χ^2-test), which is consistent with the normal motor coordination observed in PTPMEG-KO mice. We also examined the kinetics and short-term plasticity of EPSCs elicited by stimulation of mono-innervating CFs. The 10–90% rise times, decay time constants and chord conductance calculated between the holding potential of −10 mV and +50 mV were similar between wild-type and PTPMEG-KO mice (data not shown). The paired-pulse depression of CF-EPSCs was also similar between wild-type and PTPMEG-KO mice (Fig. 5B). Therefore, it is likely that the CF-mediated calcium entry, which is critical for the induction of LTD at PF–PC synapses (Sakurai, 1990; Konnerth *et al.*, 1992), would be normal in PTPMEG-KO PCs. Next, we examined whether the PF synaptic transmission was affected in PTPMEG-KO mice. We stimulated PFs at different intensities, and amplitudes of PF-EPSCs were plotted as a function of stimulus intensities. As shown in Fig. 6A, the slopes of the amplitude–intensity curves were similar between wild-type and PTPMEG-KO PCs ($P > 0.05$, *t*-test). Furthermore, the 10–90% rise times and decay time constants in PF-EPSCs and the paired-pulse facilitation of PF-EPSCs were indistinguishable between wild-type and PTPMEG-KO mice (Fig. 6B). These results suggest that the developmental elimination of surplus CFs and the physiological properties of excitatory synaptic inputs to PCs are basically normal in PTPMEG-KO mice.

Impairment of cerebellar LTD in PTPMEG-KO mice

We next examined whether the lack of PTPMEG affected cerebellar LTD at PF–PC synapses. After stable recordings of PF-EPSCs for 10 min, LTD was induced by a conventional conjunction protocol, which consisted of 300 single PF stimuli in conjunction with a depolarizing pulse repeated at 1 Hz. In wild-type mice, LTD was readily induced by the conjunctive stimulation (Fig. 7A). At 21–30 min after the conditioning, the mean amplitude of EPSCs elicited by PF stimulation was reduced to 61.9 ± 2.1% (mean ± SEM) of the control value measured prior to the conjunctive stimulation (Fig. 7B). The same conjunctive stimulation also induced LTD in PTPMEG-KO mice. However, the mean value of the EPSC amplitude at 21–30 min after the conditioning (76.8 ± 2.4%) was significantly higher ($P = 0.00038$, *t*-test) than the wild-type value (Fig. 7A and B). Therefore, cerebellar LTD was present but impaired in PTPMEG-KO mice, suggesting that PTPMEG-mediated tyrosine dephosphorylation events have a modulatory role in cerebellar LTD.

Discussion

In this study, we demonstrated that PTPMEG-KO mice showed impairment in motor learning and cerebellar LTD. To our knowledge, mice devoid of a PTK or a PTP that show defects in cerebellar LTD and motor learning have not been reported.

PTPMEG belongs to a subfamily of cytoplasmic PTPs that contains FERM and catalytic PTP domains (Alonso *et al.*, 2004). This PTP

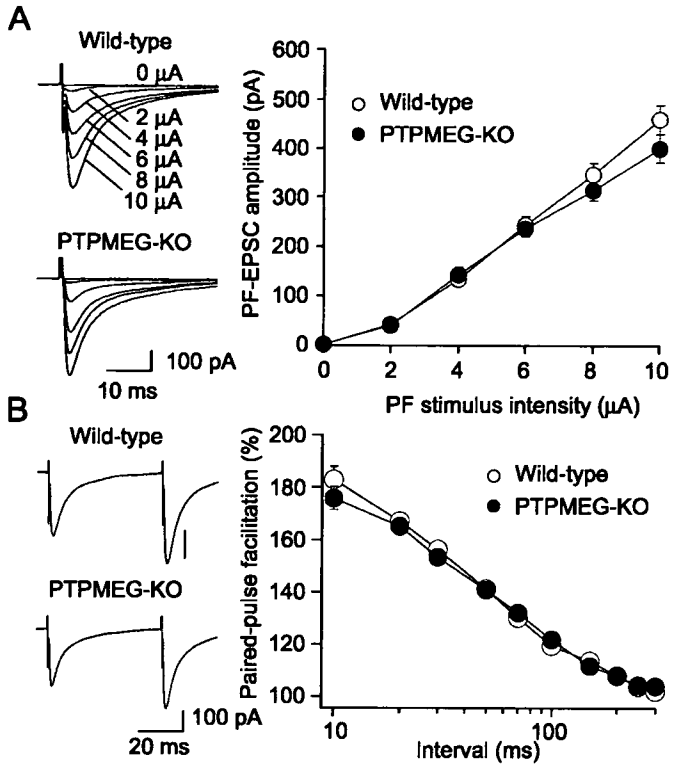

FIG. 6. Normal excitatory synaptic transmission in the parallel fiber (PF)–PC synapses of PTPMEG-knockout (KO) mice. (A) Input–output relationship of the PF-excitatory postsynaptic currents (EPSCs). (left) Representative traces of PF-EPSCs with increasing stimulus intensities (0–10 μA) recorded from wild-type (top) and PTPMEG-KO (bottom) PCs. (right) Amplitudes of PF-EPSCs plotted as a function of stimulus intensities in the wild-type (open circles, $n = 26$) and PTPMEG-KO (closed circles, $n = 19$) PCs. Each point represents the mean ± SEM. There was no significant difference between wild-type and PTPMEG-KO mice ($P > 0.05$, t-test). (B) Short-term synaptic plasticity of PF-EPSCs. (left) Representative traces of PF-EPSCs evoked by paired pulses at an interpulse interval of 50 ms. Ten traces were averaged. (right) Summary graph showing paired-pulse facilitation of PF-EPSCs in wild-type (open circles, $n = 17$) and PTPMEG-KO (closed circles, $n = 20$) PCs. The amplitude of the second response is expressed as a percentage of the first response (mean ± SEM) and is plotted as a function of interpulse intervals. There was no significant difference between wild-type and PTPMEG-KO mice. Stimulus pairs were applied at 0.5 Hz. The holding potential was −80 mV.

family consists of PTPMEG, PTPH1/PTPN3, PTPD1/PTPN21, PTPD2/PTPN14 and PTP-BL/PTPN13. In addition, three PTPs of this family have one (PTPMEG and PTPH1) or five (PTP-BL) PDZ domains. PTPH1 is the closest homolog of PTPMEG (Yang & Tonks, 1991). Mice lacking PTP-BL phosphatase activity are mildly impaired in motor nerve repair after sciatic nerve lesions (Wansink *et al.*, 2004). Mice lacking PTPH1 phosphatase activity show normal signal transduction upon stimulation of T-cell antigen receptors (Bauler *et al.*, 2007). Physiological importance of this PTP family in the mammalian CNS had not been demonstrated.

Tyrosine phosphorylation/dephosphorylation is thought to be involved in the cerebellar development, including the layer formation, CF-PC synapse elimination and PC morphology (Howell *et al.*, 2000; Meathrel *et al.*, 2002; Kakizawa *et al.*, 2003; Tanaka *et al.*, 2003). Axons of cerebellar granule cells are disorganized and tangled in mice lacking PTPσ/PTPRS, a receptor-type PTP (Meathrel *et al.*, 2002). Signaling through PTPζ/RPTPβ/PTPRZ1 regulates the morphogenesis of PC dendrites (Tanaka *et al.*, 2003). In addition, *Drosophila* PTPMEG is involved in the proper establishment and maintenance of axon projections in the central brain (Whited *et al.*, 2007). The expression level of PTPMEG was low during the cerebellar development, and the normal cerebellar development of PTPMEG-KO mice was grossly maintained, although subtle alterations could not be excluded. Consistently, the developmental elimination of surplus CFs of PCs normally occurred in PTPMEG-KO mice (Fig. 5A). However, other FERM-containing PTPs, especially PTPH1 that is reported to be expressed in the cerebellum (Sahin *et al.*, 1995), may compensate for the lack of PTPMEG in the mutant mice. Mice lacking both PTPMEG and PTPH1 might reveal roles of these PTPs in the cerebellar development.

We found mild, but significant, impairment in both acquisition of the cerebellum-dependent delay eyeblink conditioning and cerebellar LTD at PF–PC synapses in PTPMEG-KO mice. Cerebellar LTD was present, but attenuated, in these mice (Fig. 7). The delay eyeblink conditioning was also impaired in these mice during the early stage of acquisition (Fig. 3). These results suggest that PTPMEG-regulated tyrosine dephosphorylation events are not indispensable for, but modulate, cerebellar LTD and motor learning. Alternatively, other PTPs such as PTPH1 may also contribute to cerebellar synaptic plasticity. It would be obviously important to further clarify roles of PTPMEG and the related PTPs in the adult cerebellum.

Cellular mechanisms underlying defects in motor learning in PTPMEG-KO mice

Many previous studies strongly suggest that LTD at PF–PC synapses underlies motor learning in the cerebellum (Ito, 2001). Several mutant mice that have defects in LTD show impairment in the delay eyeblink conditioning. These mouse models include mice lacking mGluR1 (Aiba *et al.*, 1994; Kishimoto *et al.*, 2002), GluRδ2 (Kishimoto *et al.*, 2001c), phospholipase Cβ4 (Kishimoto *et al.*, 2001a; Miyata *et al.*, 2001) and CB1 cannabinoid receptors (Safo & Regehr, 2005; Kishimoto & Kano, 2006). In these four mutant mice, the defects are more severe than those in PTPMEG-KO mice: cerebellar LTD is deficient, and the sustained levels of CR% in the delay eyeblink conditioning are severely impaired. In addition, both LTD and delay eyeblink conditioning are restored in mGluR1-rescue mice in which mGluR1α is expressed only in PCs in mGluR1-KO mice by using a PC-specific promoter (Ichise *et al.*, 2000; Kishimoto *et al.*, 2002). These findings are consistent with the notion that cerebellar LTD is a cellular substrate of the delay eyeblink conditioning. Therefore, it is likely that impairment in LTD is a cause of impaired acquisition of the delay eyeblink conditioning in PTPMEG-KO mice. To support this idea, the sustained level of CR% was comparable between wild-type and PTPMEG-KO mice, which might be explained by impaired but still significant cerebellar LTD in the absence of PTPMEG. However, PTPMEG is expressed not only in PCs, but also in the thalamus, cortex and hippocampus (Hironaka *et al.*, 2000). Therefore, we could not exclude the possibility that PTPMEG expressed in neurons other than PCs is critical for the motor-memory formation. The phenotype of PTPMEG-KO mice in the delay eyeblink conditioning bears a closer resemblance to that of GluRε1/NR2A-KO mice (Kishimoto *et al.*, 1997, 2001b), which exhibit impaired long-term potentiation (LTP) in the hippocampal CA1 region (Sakimura *et al.*, 1995). At the early stage of the delay conditioning training, GluRε1-KO mice also exhibit lower CR% and EMG amplitude, but they catch up with wild-type mice in the CR% by the end of the conditioning training (Kishimoto *et al.*, 1997, 2001c). Taking account of the fact that PTPMEG interacts not only with GluRδ2 but also with GluRε1

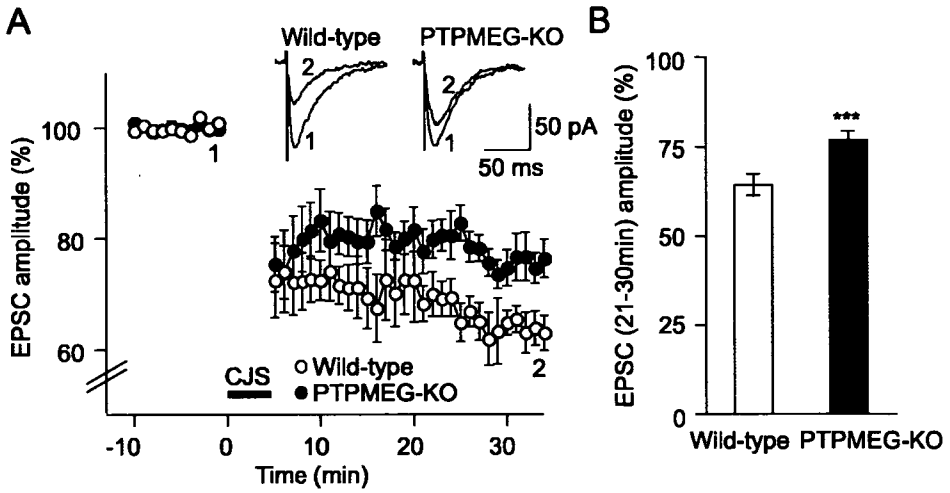

FIG. 7. Impaired cerebellar LTD in PTPMEG-knockout (KO) mice. (A) Cerebellar LTD. Summary of changes in the amplitude of PF-excitatory postsynaptic currents (EPSCs) before and after the conjunctive stimulus (CJS, solid bar) in wild-type (open circles, $n = 6$) and PTPMEG-KO (closed circles, $n = 8$) mice. The amplitude was normalized to the mean initial value recorded for 10 min before the CJS. Insets show sample traces of PF-EPSCs recorded just before (1) and 30 min after (2) the CJS. The data are expressed as the mean ± SEM. (B) The mean amplitude of PF-EPSCs at 21–30 min after the CJS in (A) in wild-type (open column, $n = 6$) and PTPMEG-KO mice (closed column, $n = 8$). The data are expressed as the mean ± SEM. ***$P = 0.00038$ (t-test).

(Hironaka *et al.*, 2000), PTPMEG expressed in other brain regions such as the hippocampus might be involved in the rapid memory formation in the eyeblink conditioning.

Molecular mechanisms of the regulation of cerebellar functions by PTPMEG

Recent studies have identified several PTKs, PTPs and their substrates that are critical for hippocampal synaptic plasticity and hippocampus-dependent learning. For example, Fyn-KO and EphB2-KO mice show impairment in hippocampal functions (Grant *et al.*, 1992; Grunwald *et al.*, 2001). PTPα/PTPRA-KO mice show impaired LTP in the hippocampal CA1 region and poor performance in the radial arm-maze and water-maze tests (Petrone *et al.*, 2003). PTPδ/PTPRD-KO mice also show learning impairment in the water-maze, reinforced T-maze and radial arm-maze tests with enhanced LTP and paired-pulse facilitation in the hippocampal CA1 region (Uetani *et al.*, 2000). PTPRZ1-KO mice show age-dependent enhancement of hippocampal LTP and impairment in the water-maze test (Niisato *et al.*, 2005). The *N*-methyl-D-aspartate (NMDA)-type glutamate receptors (NMDARs), which play pivotal roles in hippocampus-dependent spatial learning and LTP in hippocampal CA1 neurons, are regulated by their tyrosine phosphorylation status (Salter & Kalia, 2004). Currents through NMDARs are potentiated by Src-family PTKs. Tyrosine dephosphorylation of NMDARs is implicated in receptor internalization (Snyder *et al.*, 2005). In contrast, tyrosine phosphorylation of GluR2 results in its endocytosis, leading to the reduction of AMPAR-mediated currents (Ahmadian *et al.*, 2004). However, little is known about PTKs and their substrates in cerebellar synaptic plasticity. Functional NMDARs are not expressed in PCs, and the level of GluR2 tyrosine phosphorylation in the cerebellum is low (Hayashi & Huganir, 2004). Identification of the substrates of PTPMEG would clarify the mechanisms of cerebellar LTD and motor learning. Our preliminary data showed that tyrosine phosphorylation of a protein with an approximate mass of 73 kDa was elevated in the cerebellum of 8-week-old PTPMEG-KO mice (data not shown). Further characterization of the 73 kDa protein as well as other possible targets would be important.

Regulation of PTPMEG in the cerebellum is currently elusive. GluRδ2 can regulate PTPMEG, as PTPMEG binds to GluRδ2 through its PDZ domain (Hironaka *et al.*, 2000). However, GluRδ2-KO mice have severe abnormalities not only in the cerebellar LTD and delay eyeblink conditioning, but also in the PF–PC synapse formation and CF innervation pattern (Kurihara *et al.*, 1997; Hashimoto *et al.*, 2001; Ichikawa *et al.*, 2002), whereas PTPMEG-KO mice exhibited a normal CF innervation pattern (Fig. 5A). In addition, the PF–PC synapse formation would also be normal in PTPMEG-KO mice because defects in PF innervation lead to abnormal CF innervation (Hashimoto *et al.*, 2001). Indeed, PTPMEG-KO mice showed normal responses of PCs to PF stimulation (Fig. 6A). Thus, PTPMEG is not likely to be involved in the signaling cascade controlling the excitatory synapse formation on PCs. On the other hand, because the magnitude of LTD, which is completely absent in GluRδ2-KO mice, was attenuated in PTPMEG-KO mice (Fig. 7), regulation of LTD by GluRδ2 may involve PTPMEG at least partly. GluRδ2 is localized to the postsynaptic density of PF–PC synapses, which are formed on spines of distal PC dendrites (Landsend *et al.*, 1997). PTPMEG is also found in the postsynaptic density of the cerebellum (Hironaka *et al.*, 2000). Moreover, PDZ proteins that bind to the carboxyl-terminus of GluRδ2 are crucial for conveying signals necessary for the induction of LTD in cerebellar slices (Kohda *et al.*, 2007), although another report shows that the membrane-proximal but not PDZ-binding sequence in the cytoplasmic region of GluRδ2 is crucial for cerebellar LTD in cultured PCs (Yawata *et al.*, 2006). Therefore, GluRδ2 may partly function as a scaffold protein for intracellular signaling molecules such as PTPMEG (Yuzaki, 2004). In addition, it is also possible that mGluR1 regulates PTPMEG, because two PTP inhibitors, orthovanadate and phenylarsine oxide, block hippocampal LTD induced by the type I mGluR agonist (*RS*)-3,5-dihydroxyphenylglycine stimulation (Moult *et al.*, 2006). Moreover, the elevation of intracellular Ca^{2+}, which is essential for cerebellar LTD (Sakurai, 1990; Konnerth *et al.*, 1992), may also regulate PTPMEG. Calpain, a Ca^{2+}-dependent protease, is involved in the Ca^{2+}-dependent signaling pathway in PCs (Hirai, 2001). Interestingly, the phosphatase activity of PTPMEG increases when it is cleaved by calpain (Gu & Majerus, 1996), raising the possibility that PTPMEG is activated upon the

induction of cerebellar LTD. The subcellular localization and activity of PTPMEG during cerebellar LTD would be critical issues to be addressed.

Acknowledgements

We thank Drs K. Hironaka and J. Goto for their help on the generation and analysis of PTPMEG-KO mice. This research was supported in part by Grants-in-Aids for Scientific Research on Priority Areas and National Project on Protein Structural and Functional Analyses from Ministry of Education, Culture, Sports, Science and Technology of Japan.

Abbreviations

AMPAR, α-amino-3-hydroxy-5-methyl-4-isoxazolepropionic acid type receptor; CF, climbing fiber; CR, conditioned response; CS, conditioned stimulus; EMG, electromyogram; EPSC, excitatory postsynaptic current; GluR, glutamate receptor; KO, knockout; LTD, long-term depression; LTP, long-term potentiation; mGluR, metabotropic glutamate receptor; NMDA, *N*-methyl-D-aspartate; PC, Purkinje cell; PDZ, postsynaptic density-95/discs-large/ZO-1; PF, parallel fiber; PKC, protein kinase C; PTK, protein-tyrosine kinase; PTP, protein-tyrosine phosphatase; UR, unconditioned response; US, unconditioned stimulus.

References

Ahmadian, G., Ju, W., Liu, L., Wyszynski, M., Lee, S.H., Dunah, A.W., Taghibiglou, C., Wang, Y., Lu, J., Wong, T.P., Sheng, M. & Wang, Y.T. (2004) Tyrosine phosphorylation of GluR2 is required for insulin-stimulated AMPA receptor endocytosis and LTD. *EMBO J.*, **23**, 1040–1050.

Aiba, A., Kano, M., Chen, C., Stanton, M.E., Fox, G.D., Herrup, K., Zwingman, T.A. & Tonegawa, S. (1994) Deficient cerebellar long-term depression and impaired motor learning in mGluR1 mutant mice. *Cell*, **79**, 377–388.

Alonso, A., Sasin, J., Bottini, N., Friedberg, I., Friedberg, I., Osterman, A., Godzik, A., Hunter, T., Dixon, J. & Mustelin, T. (2004) Protein tyrosine phosphatases in the human genome. *Cell*, **117**, 699–711.

Bauler, T.J., Hughes, E.D., Arimura, Y., Mustelin, T., Saunders, T.L. & King, P.D. (2007) Normal TCR signal transduction in mice that lack catalytically active PTPN3 protein tyrosine phosphatase. *J. Immunol.*, **178**, 3680–3687.

Boxall, A.R., Lancaster, B. & Garthwaite, J. (1996) Tyrosine kinase is required for long-term depression in the cerebellum. *Neuron*, **16**, 805–813.

Boyden, E.S., Katoh, A. & Raymond, J.L. (2004) Cerebellum-dependent learning: the role of multiple plasticity mechanisms. *Annu. Rev. Neurosci.*, **27**, 581–609.

Callahan, C.A. & Thomas, J.B. (1994) Tau-β-galactosidase, an axon-targeted fusion protein. *Proc. Natl Acad. Sci. USA*, **91**, 5972–5976.

Castro-Alamancos, M.A. & Torres-Aleman, I. (1994) Learning of the conditioned eye-blink response is impaired by an antisense insulin-like growth factor I oligonucleotide. *Proc. Natl Acad. Sci. USA*, **91**, 10203–10207.

Chen, L., Bao, S., Lockard, J.M., Kim, J.K. & Thompson, R.F. (1996) Impaired classical eyeblink conditioning in cerebellar-lesioned and Purkinje cell degeneration (pcd) mutant mice. *J. Neurosci.*, **16**, 2829–2838.

Chung, H.J., Steinberg, J.P., Huganir, R.L. & Linden, D.J. (2003) Requirement of AMPA receptor GluR2 phosphorylation for cerebellar long-term depression. *Science*, **300**, 1751–1755.

Fujiwara, A., Kakizawa, S. & Iino, M. (2007) Induction of cerebellar long-term depression requires activation of calcineurin in Purkinje cells. *Neuropharmacology*, **52**, 1663–1670.

Granon, S., Faure, P. & Changeux, J.P. (2003) Executive and social behaviors under nicotinic receptor regulation. *Proc. Natl Acad. Sci. USA*, **100**, 9596–9601.

Grant, S.G., O'Dell, T.J., Karl, K.A., Stein, P.L., Soriano, P. & Kandel, E.R. (1992) Impaired long-term potentiation, spatial learning, and hippocampal development in fyn mutant mice. *Science*, **258**, 1903–1910.

Grunwald, I.C., Korte, M., Wolfer, D., Wilkinson, G.A., Unsicker, K., Lipp, H.P., Bonhoeffer, T. & Klein, R. (2001) Kinase-independent requirement of EphB2 receptors in hippocampal synaptic plasticity. *Neuron*, **32**, 1027–1040.

Gu, M. & Majerus, P.W. (1996) The properties of the protein tyrosine phosphatase PTPMEG. *J. Biol. Chem.*, **271**, 27751–27759.

Gu, M., Meng, K. & Majerus, P.W. (1996) The effect of overexpression of the protein tyrosine phosphatase PTPMEG on cell growth and on colony formation in soft agar in COS-7 cells. *Proc. Natl Acad. Sci. USA*, **93**, 12980–12985.

Gu, M.X., York, J.D., Warshawsky, I. & Majerus, P.W. (1991) Identification, cloning, and expression of a cytosolic megakaryocyte protein-tyrosine-phosphatase with sequence homology to cytoskeletal protein 4.1. *Proc. Natl Acad. Sci. USA*, **88**, 5867–5871.

Hashimoto, K., Ichikawa, R., Takechi, H., Inoue, Y., Aiba, A., Sakimura, K., Mishina, M., Hashikawa, T., Konnerth, A., Watanabe, M. & Kano, M. (2001) Roles of glutamate receptor δ2 subunit (GluRδ2) and metabotropic glutamate receptor subtype 1 (mGluR1) in climbing fiber synapse elimination during postnatal cerebellar development. *J. Neurosci.*, **21**, 9701–9712.

Hashimoto, K. & Kano, M. (2005) Postnatal development and synapse elimination of climbing fiber to Purkinje cell projection in the cerebellum. *Neurosci. Res.*, **53**, 221–228.

Hayashi, T. & Huganir, R.L. (2004) Tyrosine phosphorylation and regulation of the AMPA receptor by SRC family tyrosine kinases. *J. Neurosci.*, **24**, 6152–6160.

Hirai, H. (2001) Ca^{2+}-dependent regulation of synaptic δ2 glutamate receptor density in cultured rat Purkinje neurons. *Eur. J. Neurosci.*, **14**, 73–82.

Hirai, H., Launey, T., Mikawa, S., Torashima, T., Yanagihara, D., Kasaura, T., Miyamoto, A. & Yuzaki, M. (2003) New role of δ2-glutamate receptors in AMPA receptor trafficking and cerebellar function. *Nat. Neurosci.*, **6**, 869–876.

Hironaka, K., Umemori, H., Tezuka, T., Mishina, M. & Yamamoto, T. (2000) The protein-tyrosine phosphatase PTPMEG interacts with glutamate receptor δ2 and ε subunits. *J. Biol. Chem.*, **275**, 16167–16173.

Howell, B.W., Herrick, T.M., Hildebrand, J.D., Zhang, Y. & Cooper, J.A. (2000) Dab1 tyrosine phosphorylation sites relay positional signals during mouse brain development. *Curr. Biol.*, **10**, 877–885.

Ichikawa, R., Miyazaki, T., Kano, M., Hashikawa, T., Tatsumi, H., Sakimura, K., Mishina, M., Inoue, Y. & Watanabe, M. (2002) Distal extension of climbing fiber territory and multiple innervation caused by aberrant wiring to adjacent spiny branchlets in cerebellar Purkinje cells lacking glutamate receptor δ2. *J. Neurosci.*, **22**, 8487–8503.

Ichise, T., Kano, M., Hashimoto, K., Yanagihara, D., Nakao, K., Shigemoto, R., Katsuki, M. & Aiba, A. (2000) mGluR1 in cerebellar Purkinje cells essential for long-term depression, synapse elimination, and motor coordination. *Science*, **288**, 1832–1835.

Ito, M. (2001) Cerebellar long-term depression: characterization, signal transduction, and functional roles. *Physiol. Rev.*, **81**, 1143–1195.

Ito, M. (2002) The molecular organization of cerebellar long-term depression. *Nat. Rev. Neurosci.*, **3**, 896–902.

Kadotani, H., Hirano, T., Masugi, M., Nakamura, K., Nakao, K., Katsuki, M. & Nakanishi, S. (1996) Motor discoordination results from combined gene disruption of the NMDA receptor NR2A and NR2C subunits, but not from single disruption of the NR2A or NR2C subunit. *J. Neurosci.*, **16**, 7859–7867.

Kakizawa, S., Kishimoto, Y., Hashimoto, K., Miyazaki, T., Furutani, K., Shimizu, H., Fukaya, M., Nishi, M., Sakagami, H., Ikeda, A., Kondo, H., Kano, M., Watanabe, M., Iino, M. & Takeshima, H. (2007) Junctophilin-mediated channel crosstalk essential for cerebellar synaptic plasticity. *EMBO J.*, **26**, 1924–1933.

Kakizawa, S., Yamada, K., Iino, M., Watanabe, M. & Kano, M. (2003) Effects of insulin-like growth factor I on climbing fibre synapse elimination during cerebellar development. *Eur. J. Neurosci.*, **17**, 545–554.

Kano, M., Hashimoto, K., Chen, C., Abeliovich, A., Aiba, A., Kurihara, H., Watanabe, M., Inoue, Y. & Tonegawa, S. (1995) Impaired synapse elimination during cerebellar development in PKCγ mutant mice. *Cell*, **83**, 1223–1231.

Kashiwabuchi, N., Ikeda, K., Araki, K., Hirano, T., Shibuki, K., Takayama, C., Inoue, Y., Kutsuwada, T., Yagi, T., Kang, Y., Aizawa, S. & Mishina, M. (1995) Impairment of motor coordination, Purkinje cell synapse formation, and cerebellar long-term depression in GluRδ2 mutant mice. *Cell*, **81**, 245–252.

Kishimoto, Y., Fujimichi, R., Araishi, K., Kawahara, S., Kano, M., Aiba, A. & Kirino, Y. (2002) mGluR1 in cerebellar Purkinje cells is required for normal association of temporally contiguous stimuli in classical conditioning. *Eur. J. Neurosci.*, **16**, 2416–2424.

Kishimoto, Y., Hirono, M., Sugiyama, T., Kawahara, S., Nakao, K., Kishio, M., Katsuki, M., Yoshioka, T. & Kirino, Y. (2001a) Impaired delay but normal trace eyeblink conditioning in PLCβ4 mutant mice. *Neuroreport*, **12**, 2919–2922.

Kishimoto, Y. & Kano, M. (2006) Endogenous cannabinoid signaling through the CB1 receptor is essential for cerebellum-dependent discrete motor learning. *J. Neurosci.*, **26**, 8829–8837.

Kishimoto, Y., Kawahara, S., Kirino, Y., Kadotani, H., Nakamura, Y., Ikeda, M. & Yoshioka, T. (1997) Conditioned eyeblink response is impaired in mutant mice lacking NMDA receptor subunit NR2A. *Neuroreport*, **8**, 3717–3721.

Kishimoto, Y., Kawahara, S., Mori, H., Mishina, M. & Kirino, Y. (2001b) Long-trace interval eyeblink conditioning is impaired in mutant mice lacking the NMDA receptor subunit ε1. *Eur. J. Neurosci.*, **13**, 1221–1227.

Kishimoto, Y., Kawahara, S., Suzuki, M., Mori, H., Mishina, M. & Kirino, Y. (2001c) Classical eyeblink conditioning in glutamate receptor subunit δ2 mutant mice is impaired in the delay paradigm but not in the trace paradigm. *Eur. J. Neurosci.*, **13**, 1249–1253.

Kohda, K., Kakegawa, W., Matsuda, S., Nakagami, R., Kakiya, N. & Yuzaki, M. (2007) The extreme C-terminus of GluRδ2 is essential for induction of long-term depression in cerebellar slices. *Eur. J. Neurosci.*, **25**, 1357–1362.

Konnerth, A., Dreessen, J. & Augustine, G.J. (1992) Brief dendritic calcium signals initiate long-lasting synaptic depression in cerebellar Purkinje cells. *Proc. Natl Acad. Sci. USA*, **89**, 7051–7055.

Kurihara, H., Hashimoto, K., Kano, M., Takayama, C., Sakimura, K., Mishina, M., Inoue, Y. & Watanabe, M. (1997) Impaired parallel fiber → Purkinje cell synapse stabilization during cerebellar development of mutant mice lacking the glutamate receptor δ2 subunit. *J. Neurosci.*, **17**, 9613–9623.

Landsend, A.S., Amiry-Moghaddam, M., Matsubara, A., Bergersen, L., Usami, S., Wenthold, R.J. & Ottersen, O.P. (1997) Differential localization of δ glutamate receptors in the rat cerebellum: coexpression with AMPA receptors in parallel fiber-spine synapses and absence from climbing fiber-spine synapses. *J. Neurosci.*, **17**, 834–842.

McCormick, D.A. & Thompson, R.F. (1984) Cerebellum: essential involvement in the classically conditioned eyelid response. *Science*, **223**, 296–299.

Meathrel, K., Adamek, T., Batt, J., Rotin, D. & Doering, L.C. (2002) Protein tyrosine phosphatase σ-deficient mice show aberrant cytoarchitecture and structural abnormalities in the central nervous system. *J. Neurosci. Res.*, **70**, 24–35.

Miyakawa, T., Yared, E., Pak, J.H., Huang, F.L., Huang, K.P. & Crawley, J.N. (2001) Neurogranin null mutant mice display performance deficits on spatial learning tasks with anxiety related components. *Hippocampus*, **11**, 763–775.

Miyata, M., Kim, H.T., Hashimoto, K., Lee, T.K., Cho, S.Y., Jiang, H., Wu, Y., Jun, K., Wu, D., Kano, M. & Shin, H.S. (2001) Deficient long-term synaptic depression in the rostral cerebellum correlated with impaired motor learning in phospholipase Cβ4 mutant mice. *Eur. J. Neurosci.*, **13**, 1945–1954.

Moult, P.R., Gladding, C.M., Sanderson, T.M., Fitzjohn, S.M., Bashir, Z.I., Molnar, E. & Collingridge, G.L. (2006) Tyrosine phosphatases regulate AMPA receptor trafficking during metabotropic glutamate receptor-mediated long-term depression. *J. Neurosci.*, **26**, 2544–2554.

Namiki, S., Kakizawa, S., Hirose, K. & Iino, M. (2005) NO signalling decodes frequency of neuronal activity and generates synapse-specific plasticity in mouse cerebellum. *J. Physiol.*, **566**, 849–863.

Niisato, K., Fujikawa, A., Komai, S., Shintani, T., Watanabe, E., Sakaguchi, G., Katsuura, G., Manabe, T. & Noda, M. (2005) Age-dependent enhancement of hippocampal long-term potentiation and impairment of spatial learning through the Rho-associated kinase pathway in protein tyrosine phosphatase receptor type Z-deficient mice. *J. Neurosci.*, **25**, 1081–1088.

Nolan, M.F., Malleret, G., Lee, K.H., Gibbs, E., Dudman, J.T., Santoro, B., Yin, D., Thompson, R.F., Siegelbaum, S.A., Kandel, E.R. & Morozov, A. (2003) The hyperpolarization-activated HCN1 channel is important for motor learning and neuronal integration by cerebellar Purkinje cells. *Cell*, **115**, 551–564.

Petrone, A., Battaglia, F., Wang, C., Dusa, A., Su, J., Zagzag, D., Bianchi, R., Casaccia-Bonnefil, P., Arancio, O. & Sap, J. (2003) Receptor protein tyrosine phosphatase α is essential for hippocampal neuronal migration and long-term potentiation. *EMBO J.*, **22**, 4121–4131.

Safo, P.K. & Regehr, W.G. (2005) Endocannabinoids control the induction of cerebellar LTD. *Neuron*, **48**, 647–659.

Sahin, M., Slaugenhaupt, S.A., Gusella, J.F. & Hockfield, S. (1995) Expression of PTPH1, a rat protein tyrosine phosphatase, is restricted to the derivatives of a specific diencephalic segment. *Proc. Natl Acad. Sci. USA*, **92**, 7859–7863.

Sakimura, K., Kutsuwada, T., Ito, I., Manabe, T., Takayama, C., Kushiya, E., Yagi, T., Aizawa, S., Inoue, Y., Sugiyama, H. & Mishina, M. (1995) Reduced hippocampal LTP and spatial learning in mice lacking NMDA receptor ε1 subunit. *Nature*, **373**, 151–155.

Sakurai, M. (1990) Calcium is an intracellular mediator of the climbing fiber in induction of cerebellar long-term depression. *Proc. Natl Acad. Sci. USA*, **87**, 3383–3385.

Salter, M.W. & Kalia, L.V. (2004) Src kinases: a hub for NMDA receptor regulation. *Nat. Rev. Neurosci.*, **5**, 317–328.

Schmahmann, J.D. & Sherman, J.C. (1998) The cerebellar cognitive affective syndrome. *Brain*, **121**, 561–579.

Snyder, E.M., Nong, Y., Almeida, C.G., Paul, S., Moran, T., Choi, E.Y., Nairn, A.C., Salter, M.W., Lombroso, P.J., Gouras, G.K. & Greengard, P. (2005) Regulation of NMDA receptor trafficking by amyloid-β. *Nat. Neurosci.*, **8**, 1051–1058.

Steinberg, J.P., Takamiya, K., Shen, Y., Xia, J. & Rubio, M.E., Yu, S., Jin, W., Thomas, G.M., Linden, D.J. & Huganir, R.L. (2006) Targeted in vivo mutations of the AMPA receptor subunit GluR2 and its interacting protein PICK1 eliminate cerebellar long-term depression. *Neuron*, **49**, 845–860.

Swinny, J.D., van der Want, J.J. & Gramsbergen, A. (2005) Cerebellar development and plasticity: perspectives for motor coordination strategies, for motor skills, and for therapy. *Neural Plast.*, **12**, 153–160.

Tanaka, M., Maeda, N., Noda, M. & Marunouchi, T. (2003) A chondroitin sulfate proteoglycan PTPζ/RPTPβ regulates the morphogenesis of Purkinje cell dendrites in the developing cerebellum. *J. Neurosci.*, **23**, 2804–2814.

Thompson, R.F., Bao, S., Chen, L., Cipriano, B.D., Grethe, J.S., Kim, J.J., Thompson, J.K., Tracy, J.A., Weninger, M.S. & Krupa, D.J. (1997) Associative learning. *Int. Rev. Neurobiol.*, **41**, 151–189.

Thompson, R.F. & Kim, J.J. (1996) Memory systems in the brain and localization of a memory. *Proc. Natl Acad. Sci. USA*, **93**, 13438–13444.

Uetani, N., Kato, K., Ogura, H., Mizuno, K., Kawano, K., Mikoshiba, K., Yakura, H., Asano, M. & Iwakura, Y. (2000) Impaired learning with enhanced hippocampal long-term potentiation in PTPδ-deficient mice. *EMBO J.*, **19**, 2775–2785.

Wang, Y.T. & Linden, D.J. (2000) Expression of cerebellar long-term depression requires postsynaptic clathrin-mediated endocytosis. *Neuron*, **25**, 635–647.

Wansink, D.G., Peters, W., Schaafsma, I., Sutmuller, R.P., Oerlemans, F., Adema, G.J., Wieringa, B., van der Zee, C.E. & Hendriks, W. (2004) Mild impairment of motor nerve repair in mice lacking PTP-BL tyrosine phosphatase activity. *Physiol. Genomics*, **19**, 50–60.

Whited, J.L., Robichaux, M.B., Yang, J.C. & Garrity, P.A. (2007) Ptpmeg is required for the proper establishment and maintenance of axon projections in the central brain of Drosophila. *Development*, **134**, 43–53.

Yang, Q. & Tonks, N.K. (1991) Isolation of a cDNA clone encoding a human protein-tyrosine phosphatase with homology to the cytoskeletal-associated proteins band 4.1, ezrin, and talin. *Proc. Natl Acad. Sci. USA*, **88**, 5949–5953.

Yawata, S., Tsuchida, H., Kengaku, M. & Hirano, T. (2006) Membrane-proximal region of glutamate receptor δ2 subunit is critical for long-term depression and interaction with protein interacting with C kinase 1 in a cerebellar Purkinje neuron. *J. Neurosci.*, **26**, 3626–3633.

Yuzaki, M. (2004) The δ2 glutamate receptor: a key molecule controlling synaptic plasticity and structure in Purkinje cells. *Cerebellum*, **3**, 89–93.

Melanocortin 2 receptor is required for adrenal gland development, steroidogenesis, and neonatal gluconeogenesis

Dai Chida[a,b,c], Shinichi Nakagawa[d], So Nagai[e], Hiroshi Sagara[f], Harumi Katsumata[g], Toshihiro Imaki[g], Harumi Suzuki[b], Fumiko Mitani[h], Tadashi Ogishima[i], Chikara Shimizu[e], Hayato Kotaki[a], Shigeru Kakuta[a], Katsuko Sudo[a,j], Takao Koike[e], Mitsumasa Kubo[k,l], and Yoichiro Iwakura[a]

[a]Division of Cell Biology, Center for Experimental Medicine, and [f]Fine Morphology Laboratory, Department of Basic Medical Science, Institute of Medical Science, University of Tokyo, 4-6-1, Shirokanedai, Minato-ku, Tokyo 108-8639, Japan; [b]Department of Pathology, Research Institute, International Medical Center of Japan, 1-21-1, Toyama, Shinjuku-ku, Tokyo 162-8655, Japan; [d]Nakagawa Initiative Research Unit, Initiative Research Program, Frontier Research System, RIKEN, 2-1, Hirosawa, Wako, Saitama 351-0198, Japan; [e]Department of Medicine II, Hokkaido University Graduate School of Medicine, Kita 15, Nishi 7, Kita-ku, Sapporo 060-8638, Japan; [g]Department of Bioregulation, Institute of Development and Aging Sciences, Nippon Medical School, 1-396, Kosugi-cho, Nakahara-ku, Kawasaki-city, Kanagawa 211-8533, Japan; [h]Department of Biochemistry and Integrative Medical Biology, School of Medicine, Keio University, 35 Shinanomachi, Shinjuku-ku, Tokyo 160-8582, Japan; [i]Department of Chemistry, Faculty of Sciences, Kyushu University, Hakozaki 6-10-1, Higashi-ku, Fukuoka 812-8581, Japan; [j]Animal Research Center, Tokyo Medical University, 6-1-1, Shinjuku, Shinjuku-ku, Tokyo 160-8402, Japan; and [k]Health Administration Center, Hokkaido University of Education, 5-3-1, Ainosato, Kita-ku, Sapporo 002-8501, Japan

Edited by Richard D. Palmiter, University of Washington School of Medicine, Seattle, WA, and approved September 21, 2007 (received for review July 25, 2007)

ACTH (i.e., corticotropin) is the principal regulator of the hypothalamus–pituitary–adrenal axis and stimulates steroidogenesis in the adrenal gland via the specific cell-surface melanocortin 2 receptor (MC2R). Here, we generated mice with an inactivation mutation of the MC2R gene to elucidate the roles of MC2R in adrenal development, steroidogenesis, and carbohydrate metabolism. These mice, the last of the knockout (KO) mice to be generated for melanocortin family receptors, provide the opportunity to compare the phenotype of proopiomelanocortin KO mice with that of MC1R–MC5R KO mice. We found that the MC2R KO mutation led to neonatal lethality in three-quarters of the mice, possibly as a result of hypoglycemia. Those surviving to adulthood exhibited macroscopically detectable adrenal glands with markedly atrophied zona fasciculata, whereas the zona glomerulosa and the medulla remained fairly intact. Mutations of MC2R have been reported to be responsible for 25% of familial glucocorticoid deficiency (FGD) cases. Adult MC2R KO mice resembled FGD patients in several aspects, such as undetectable levels of corticosterone despite high levels of ACTH, unresponsiveness to ACTH, and hypoglycemia after prolonged (36 h) fasting. However, MC2R KO mice differ from patients with MC2R-null mutations in several aspects, such as low aldosterone levels and unaltered body length. These results indicate that MC2R is required for postnatal adrenal development and adrenal steroidogenesis and that MC2R KO mice provide a useful animal model by which to study FGD.

adrenocorticotropic hormone (ACTH) | familial glucocorticoid deficiency (FGD) | hypothalamus–pituitary–adrenal | zona fasciculata

The adrenal gland regulates a number of essential physiological functions in adult organisms through the production of steroids and catecholamines. Maintenance of adrenal structure and function is regulated through the integration of extra- and intracellular signals. The pituitary hormone ACTH (i.e., adrenocorticotropic hormone), which is derived from the proopiomelanocortin (POMC) polypeptide precursor, is the principal regulator that stimulates adrenal glucocorticoid (GC) biosynthesis and secretion via the membrane-bound specific receptor for ACTH, ACTH receptor/melanocortin 2 receptor (MC2R) (1).

It was previously demonstrated that, although POMC knockout (KO) mice are born at the expected Mendelian frequency, three-quarters of POMC KO mice undergo neonatal death. Furthermore, those mice surviving to adulthood exhibit obesity, pigmentation defects, and adrenal insufficiency (2–4). POMC KO mice possess macroscopically detectable adrenal glands that lack normal architecture (2, 4, 5). These results demonstrate the importance of POMC-derived peptides in regulating the hypothalamus–pituitary–adrenal axis and adrenal development.

Familial glucocorticoid deficiency (FGD), or hereditary unresponsiveness to ACTH [Online Mendelian Inheritance in Man (OMIM) no. 202200; www.ncbi.nlm.nih.gov/entrez/dispomim.cgi?id=202200], is an autosomal recessive disorder resulting from resistance to the action of ACTH on the adrenal cortex. Affected individuals are deficient in cortisol and, if untreated, are likely to die as a result of hypoglycemia or overwhelming infection in infancy or childhood (6). Mutations of MC2R are responsible for 25% of FGD cases. Mutations of the MC2R accessory protein MRAP, which plays a role in the trafficking of MC2R from the endoplasmic reticulum to the cell surface, account for 20% of FGD cases (7), and a third locus responsible for FGD has been suggested (8). There has been no animal model for FGD, and MC2R KO mice are likely to become a valuable tool for the pathophysiological investigation of FGD.

To study specifically the roles of MC2R in adrenal gland development, steroidogenesis, and carbohydrate metabolism, we generated mice with an inactivation mutation of the MC2R gene. We demonstrated that disruption of MC2R leads to neonatal lethality in approximately three-quarters of MC2R KO pups, possibly as a result of hypoglycemia. Those surviving to adulthood exhibited macroscopically detectable adrenal glands with markedly atrophied zona fasciculata (zF) and lack of detectable levels of GC and reduced serum concentrations of aldosterone and epinephrine. Those surviving to adulthood exhibited hypoglycemia after prolonged (36 h) fasting as a result of the reduced expression of the genes involved in gluconeogenesis.

Author contributions: D.C., T.K., M.K., and Y.I. designed research; D.C., S. Nakagawa, S. Nagai, H. Sagara, H. Katsumata, T.I., C.S., H. Kotaki, S.K., K.S., and M.K. performed research; H. Suzuki, F.M., and T.O. contributed new reagents/analytic tools; D.C., S. Nakagawa, H. Sagara, T.I., F.M., M.K., and Y.I. analyzed data; and D.C. and M.K. wrote the paper.

The authors declare no conflict of interest.

This article is a PNAS Direct Submission.

Abbreviations: ACTH, adrenocorticotropic hormone; POMC, proopiomelanocortin; GC, glucocorticoid; KO, knockout; FGD, familial glucocorticoid deficiency; zF, zona fasciculata; zG, zona glomerulosa; ME, medulla; TH, tyrosine hydroxylase.

[c]To whom correspondence should be sent at the b address. E-mail: dchida@ri.imcj.go.jp.

[l]Deceased January 21, 2007.

This article contains supporting information online at www.pnas.org/cgi/content/full/0706953104/DC1.

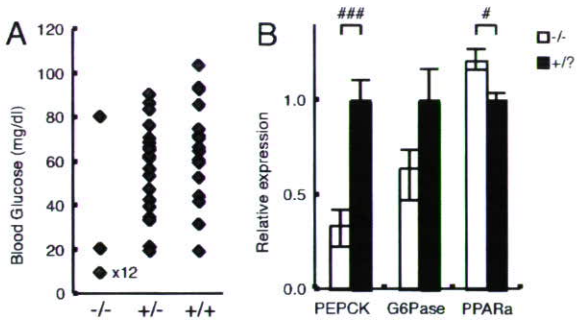

Fig. 1. Neonatal hypoglycemia in MC2R KO mice. (*A*) Blood glucose levels on postnatal day 0.5 at 1200 hours. Detection limit was 20 mg/dl. Each point indicates the glucose level of a single pup. The blood glucose level of 12 of 14 homozygous pups was under detection level (<20 mg/dl). The values below detection level were plotted at 10 mg/dl. (*B*) MC2R pups were killed at 1200 hours, and liver RNAs were prepared. The experiments were performed with postnatal day 0.5 $MC2R^{-/-}$ ($n = 6$) and $MC2R^{+/?}$ ($n = 9$) mice. The expression of phosphoenolpyruvate carboxykinase (PEPCK), glucose-6-phosphatase (G6Pase), and peroxisome proliferator-activated receptor α (PPARa) in the liver was determined by qRT-PCR. Data are expressed as means ± SEM. Statistical significance was determined by *t* test. #, $P < 0.05$.

Results

Generation of MC2R KO Mice. To generate MC2R KO mice, a targeting vector was constructed in which the portion of the MC2R gene encoding the entire coding region (9) was replaced with a neomycin-resistance gene cassette [supporting information (SI) Fig. 7*A*]. One of 545 neomycin-resistant colonies screened was positive as assessed by Southern analysis with an external probe (Fig. 7*B*). Chimeric founder mice were produced from the targeted ES cell clones, and germ-line transmission of the disrupted allele was obtained. MC2R KO mice were backcrossed to C57BL/6J mice for five generations before use in this study. To confirm the deficiency of MC2R, expression of the MC2R gene in the adrenal gland was examined by quantitative real-time PCR (qRT-PCR). No mRNA was detected in $MC2R^{-/-}$ mice, and expression was decreased by approximately half in $MC2R^{+/-}$ mice (Fig. 7*C*).

Most of the MC2R KO Pups Died Shortly After Birth. Mice that were homozygous null for MC2R were obtained by interbreeding heterozygous mice. Pups lacking MC2R were born at the expected Mendelian ratio, suggesting that MC2R is not essential for embryonic development. Of 190 mice born from heterozygous MC2R KO parents, 61 pups were dead before weaning at 4 wk of age. Genotype analysis revealed that most of the 61 dead pups were homozygous for the MC2R allele. Genotype analysis of 129 mice at 4 wk revealed 9 homozygote, 74 heterozygote, and 46 WT mice. Approximately three-quarters of MC2R KO pups died before weaning, mostly within 48 h after birth. Most of the mutant newborn mice were indistinguishable from their WT littermates; some homozygous pups were pink and had milk in their stomachs, whereas some homozygous pups were lethargic and pale.

We analyzed blood glucose levels on postnatal day 0.5 at 1200 hours. Three of 57 mice had already died at the time of analysis (two were $MC2R^{-/-}$ and one was $MC2R^{+/-}$). $MC2R^{-/-}$ pups were significantly hypoglycemic compared with $MC2R^{+/?}$ pups (Fig. 1*A*). We found only one of 14 homozygous pups that maintained normal blood glucose levels, comparable with those in WT mice. It is possible that this pup could survive neonatal death and grow to adulthood. Blood glucose levels for 12 of 14 homozygous pups were below detection level (<20 mg/dl). Analysis of blood glucose levels on postnatal day 7 revealed that $MC2R^{-/-}$ pups maintained glucose levels comparable with those of WT mice (data not shown). Expression of phosphoenolpyruvate carboxykinase (PEPCK), a rate-limiting enzyme for gluconeogenesis in liver, was significantly decreased, and expression of glucose-6-phosphatase (G6Pase) was relatively decreased in MC2R KO pups compared with $MC2R^{+/?}$ pups (Fig. 1*B*). The expression of peroxisome proliferator-activated receptor α (PPARα) responsible for β-oxidation of free fatty acids was significantly increased in MC2R KO pups (Fig. 1*B*). These results suggest that MC2R KO mice die as a result of hypoglycemia with decreased gluconeogenesis in the liver and defective neonatal nutritional adaptation. A slight increase in mortality was observed at 3–4 wk of age, due to undetermined cause(s), but no increase in mortality was observed after that period.

The body weights of 12-wk-old MC2R KO mice were indistinguishable from those of their littermates: $MC2R^{-/-}$, 28.7 ± 0.8 g ($n = 4$); and $MC2R^{+/+}$, 28.8 ± 0.6 g ($n = 5$). Whereas FGD patients with MC2R mutations exhibited increased height and POMC KO mice exhibited increased body length (10, 11), MC2R KO mice did not exhibit any significant difference in body length compared with that of their WT siblings: $MC2R^{-/-}$, 9.58 ± 0.17 cm ($n = 5$); and $MC2R^{+/?}$, 9.74 ± 0.07 cm ($n = 10$).

Adrenal Hypoplasia in MC2R KO Mice That Survived to Adulthood. In MC2R KO mice, adrenal glands were considerably reduced in size compared with those of their WT siblings: male $MC2R^{-/-}$, 0.58 ± 0.02 mg per pair of glands ($n = 4$); and $MC2R^{+/+}$, 2.24 ± 0.18 mg per pair of glands ($n = 5$). The histological analysis revealed marked hypoplasia of zF in the mutant adrenal gland (Fig. 2*A*). The number of nuclei per 50-μm-wide column in the cortical area, however, was not significantly changed: male $MC2R^{+/-}$, 138.2 ± 13.3; and $MC2R^{-/-}$, 147.7 ± 19.8, $P > 0.35$; and female $MC2R^{+/-}$, 149.7 ± 18; and $MC2R^{-/-}$, 143.8 ± 20.7, $P > 0.61$. These results indicate that the total number of nuclei in the zF was similar in MC2R KO and WT mice. Higher-magnification images revealed that, in the MC2R KO mice, the nuclei in zF were more densely packed with reduced cytoplasmic volume (Fig. 2*B*), suggesting that a decrease in cell size, but not cell number, accounted for the hypoplasia of zF. On the other hand, the zona glomerulosa (zG) and the adrenal medulla (ME) remained fairly intact as shown in the histological sections (Fig. 2*B*). To confirm this idea, we examined the expression patterns of aldosterone synthase cytochrome P450 (P450aldo) and tyrosine hydroxylase (TH), markers for zG and ME, respectively. Both of these markers were similarly expressed in WT and MC2R KO mice (Fig. 2*C*), suggesting that the cells in zG and ME had differentiated into the appropriate cell types. We also noticed that the thickness of capsule was increased in MC2R KO mice (Fig. 2*B*, brackets).

Ultrastructural examination of zF cells in MC2R KO mice revealed that the number of lipid droplets was significantly decreased and mitochondrial appearance was inactive compared with that of WT mice (Fig. 3 *B* and *D*). In contrast, zG cells in MC2R KO mice contained lipid droplets comparable with those in WT mice, and zG cells were not significantly different from those of WT mice (Fig. 3 *A* and *C*). Chromaffin cells in MC2R KO mice exhibited a marked depletion in epinephrine-storing secretory granules (data not shown), and highly vascularized connective tissue was developed in MC2R KO adrenal ME (data not shown). The H&E staining of the adrenal glands of newborn (postnatal day 0.5) MC2R KO mice was not significantly different from that of WT siblings (data not shown), suggesting that postnatal adrenal development was impaired in MC2R KO mice.

Adrenal Hormones in MC2R KO Mice. Serum corticosterone levels in MC2R KO mice were undetectable (Fig. 4*A*): male $MC2R^{-/-}$, undetectable ($n = 4$); $MC2R^{+/-}$, 72.0 ± 8.9 ng/ml ($n = 6$); and $MC2R^{+/+}$, 59.0 ± 8.6 ng/ml ($n = 5$). ACTH levels were significantly increased in MC2R KO mice (Fig. 4*B*): male $MC2R^{-/-}$, 1,394 ± 89 pg/ml ($n = 4$); $MC2R^{+/-}$, 370 ± 50 pg/ml ($n = 6$); and $MC2R^{+/+}$,

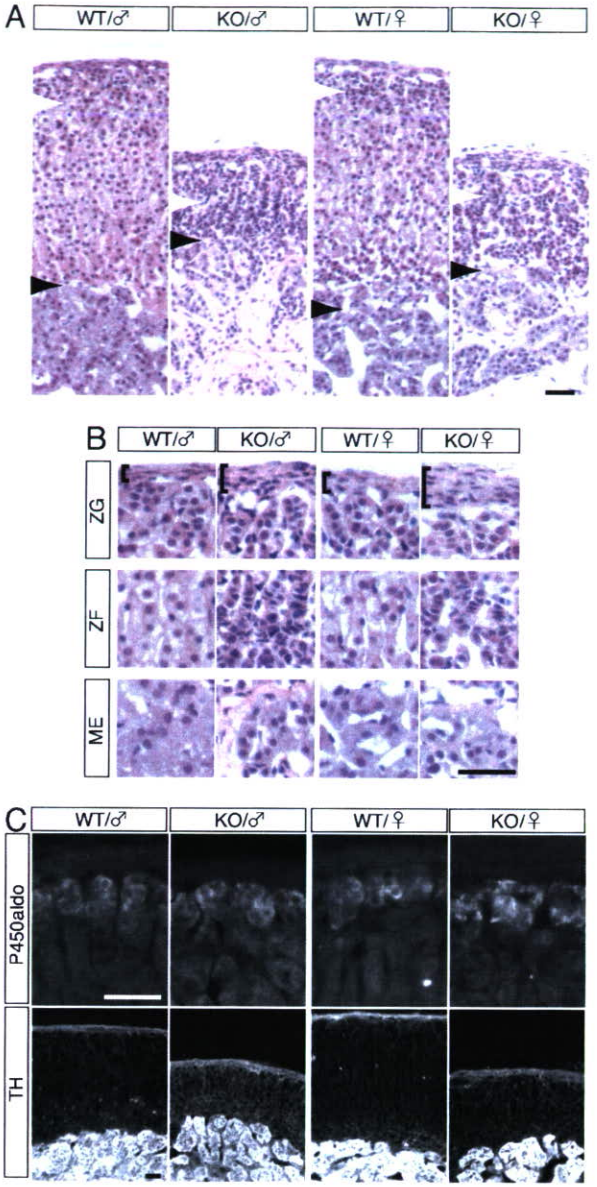

Fig. 2. Histological analysis of the adrenal gland of MC2R KO mice. (*A* and *B*) H&E staining of sections from the adrenal gland of WT or MC2R KO mice. Ten-week-old male or 13-wk-old female WT and MC2R KO mice were analyzed. (*B*) Higher-magnification images of zG, zF, and ME shown in *A*. The white and black arrowheads in *A* indicate the border between zG/zF and cortical zone/ME, respectively. The brackets in *B* indicate thickness of the capsule, which was remarkably thicker in the mutant mice. (*C*) Immunofluorescent detection of aldosterone synthase cytochrome P450 (P450aldo) and TH in the adrenal gland of WT and MC2R KO mice. Both enzymes were normally expressed in the mutant mice. (Scale bars, 50 μm.)

281 ± 106 pg/ml (n = 5). Surprisingly, serum aldosterone levels were significantly decreased in MC2R KO mice (Fig. 4*C*): male $MC2R^{-/-}$, 104 ± 25 pg/ml (n = 4); and $MC2R^{+/+}$, 343 ± 103 pg/ml (n = 5). In this regard, the MC2R-deficient mouse model is different from patients with MC2R-null mutations, in whom there is no mineralocorticoid deficiency and the renin–angiotensin system (RAS) is not affected (OMIM no. 202200). Consistent with the reduced serum corticosterone in MC2R KO mice, thymus and spleen weights were significantly increased and adipose weight was significantly decreased compared with those of WT mice (data not shown).

We analyzed the corticosterone response to exogenously

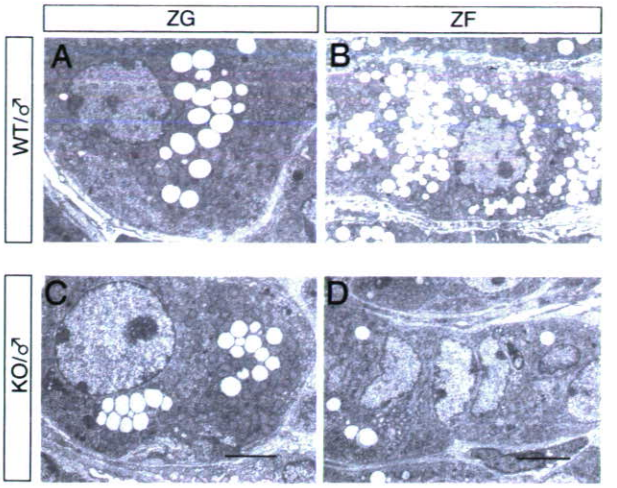

Fig. 3. Electron micrographs of the adrenal gland from MC2R KO mice. (*A* and *C*) Electron micrographs of zG of WT or MC2R KO mice. (Scale bars, 2 μm.) (*B* and *D*) Electron micrographs of zF of WT or MC2R KO mice. (Scale bars, 5 μm.) Note the remarkable decrease in lipids in zF in MC2R KO mice.

administered ACTH in MC2R KO mice. The responsiveness to ACTH was completely abrogated in MC2R KO mice (Fig. 4*E*): male $MC2R^{-/-}$, ACTH, undetectable (n = 8); $MC2R^{+/-}$, saline, 80.1 ± 13.8 ng/ml (n = 11), and ACTH, 233.9 ± 46.6 ng/ml (n = 11); and $MC2R^{+/+}$, saline, 75.2 ± 20.9 ng/ml (n = 5), and ACTH, 186.9 ± 37.6 ng/ml (n = 8). These results indicate that MC2R is essential for corticosterone release in response to ACTH.

Because ACTH plays an essential role in regulating 11β-hydroxylase (Cyp11b1) expression, as well as other genes encoding enzymes involved in steroidogenesis (12), we analyzed the expression of adrenal steroidogenic enzymes. Expression levels of cholesterol side-chain cleavage enzyme P450scc (Cyp11a1) (Fig. 5*A*), Cyp21a1 (Fig. 5*B*), and Cyp11b1 (Fig. 5*C*) were significantly reduced in MC2R KO mice, reflecting the hypoplasia of zF. The expression of Cyp11b2 [aldosterone synthase (P450aldo)] was relatively reduced in adrenal glands from MC2R KO mice (Fig. 5*D*). These results collectively indicate that the reduction of corticosterone level (Fig. 4*A*) is due to hypoplasia of zF with reduced lipid droplets (Figs. 2*A* and 3*C*), together with reduced levels of Cyp11b1 and rate-limiting Cyp11a1 (Fig. 5 *A* and *C*).

To determine the physiological effect of reduced aldosterone levels in MC2R KO mice, we measured serum electrolytes and blood pressure at 12 wk of age. There were no differences in the sodium concentrations of MC2R KO and WT mice, whereas chloride levels increased significantly in male MC2R KO mice and tended to increase in female MC2R KO mice (data not shown). Female MC2R KO mice exhibited significantly increased potassium levels (data not shown), whereas male MC2R KO mice did not. Although no significant differences in blood pressure were observed, the heart rate was significantly attenuated in MC2R KO mice (data not shown), consistent with reduced epinephrine levels in MC2R KO mice (Fig. 4*D*). We found that the expression of angiotensin receptor 1b (AT1bR) was significantly increased in MC2R KO mice (Fig. 5*E*), suggesting that renin–angiotensin system (RAS) signaling was enhanced in MC2R KO glomerulosa cells to compensate for the complete absence of ACTH signaling.

Measurement of catecholamine levels demonstrated that epinephrine levels were significantly reduced (Fig. 4*D*): male $MC2R^{-/-}$, 0.12 ± 0.02 ng/ml (n = 4); $MC2R^{+/-}$, 0.72 ± 0.14 ng/ml (n = 6); and $MC2R^{+/+}$, 0.59 ± 0.08 ng/ml (n = 5). However, norepinephrine and dopamine levels were not signif-

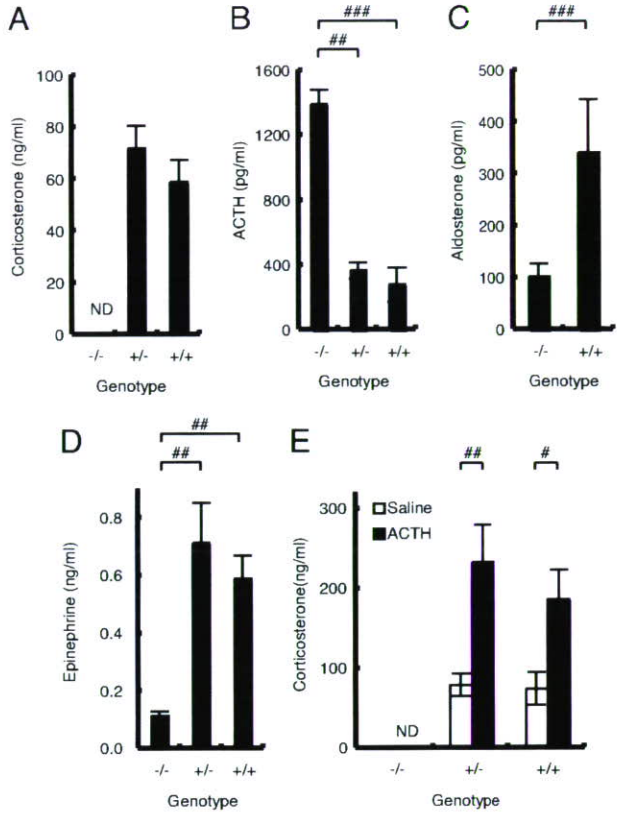

Fig. 4. Hormone levels in MC2R KO mice. (*A–D*) Blood was collected at 1600 hours from male mice (male $MC2R^{-/-}$, $n = 4$; $MC2R^{+/-}$, $n = 6$; and $MC2R^{+/+}$, $n = 5$) fasted for 8 h. Serum corticosterone (*A*), ACTH (*B*), aldosterone (*C*), and epinephrine (*D*) levels were determined. (*E*) Serum corticosterone response after ACTH (10 μg per kg of body weight) or saline injection in 12-wk-old male $MC2R^{-/-}$ [saline, not determined (ND); ACTH, $n = 8$], $MC2R^{+/-}$ (saline, $n = 11$; ACTH, $n = 11$), or $MC2R^{+/+}$ (saline, $n = 5$; ACTH, $n = 8$) mice. ACTH or saline was injected from 1000 to 1030 hours, and blood was collected after 60 min. Data are expressed as means ± SEM. Statistical significance was determined by one-way ANOVA and Fisher's protected least significant difference (PLSD) test (*A*, *B*, *D*, and *E*) or *t* test (*C*). ###, $P < 0.001$; ##, $P < 0.01$; #, $P < 0.05$.

icantly altered in MC2R KO mice (data not shown). The expression of TH was significantly reduced in MC2R KO adrenal glands (Fig. 5*F*), whereas the expression of Phox2a, a specific marker for chromaffin cells, was not significantly different (Fig. 5*G*), suggesting that MC2R is not required for chromaffin cell development but is necessary for TH expression. These results are consistent with a previous report that GC is not required for chromaffin cell development (13). We also observed that the expression of phenylethanolamine *N*-methyltransferase (PNMT), which catalyzes the conversion of norepinephrine to epinephrine and is modulated by GC, was significantly reduced in adrenal glands from MC2R KO mice (Fig. 5*H*). These results suggest that the reduced epinephrine level in MC2R KO mice is due to the reduced expression levels of PNMT and TH.

MC2R KO Mice Develop Hypoglycemia upon Prolonged Fasting. We measured blood glucose levels in animals both fed and fasted for 8 h. Interestingly, adult MC2R KO mice exhibited relatively higher glucose levels than those of WT mice under fed and 8-h fasting conditions. However, the difference was not statistically significant (data not shown). MC2R KO mice exhibited relatively reduced serum insulin levels compared with control littermates. However, the difference was not statistically significant: male $MC2R^{-/-}$, 2,044 ± 190 pg/ml ($n = 4$); and $MC2R^{+/+}$, 2,644 ± 265 pg/ml ($n = 5$).

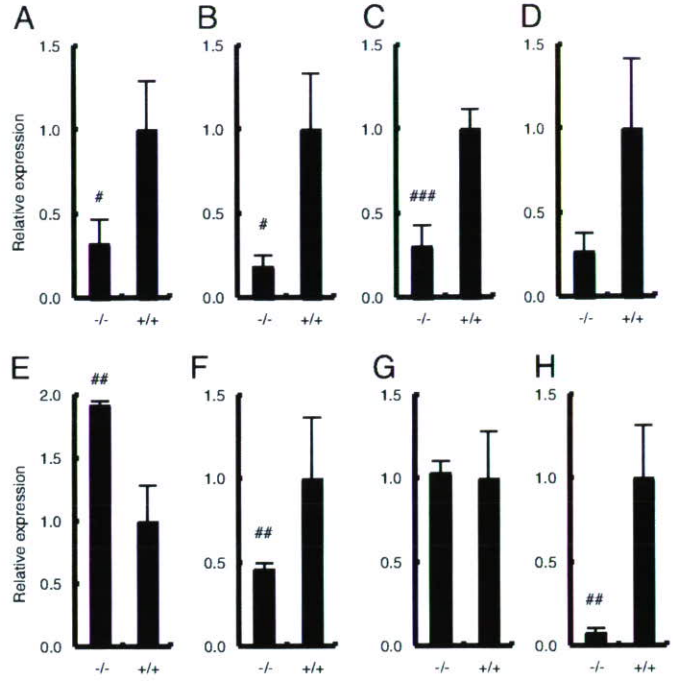

Fig. 5. Adrenal gene expression in MC2R KO mice. Expression of Cyp11a1 (*A*), Cyp21a1 (*B*), Cyp11b1 (*C*), Cyp11b2 (*D*), AT1bR (*E*), TH (*F*), Phox2a (*G*), and phenylethanolamine *N*-methyltransferase (PNMT) (*H*) in adrenal glands from female 12-wk-old $MC2R^{-/-}$ ($n = 4$) and $MC2R^{+/+}$ ($n = 3$) mice was determined by qRT-PCR. Data are expressed as means ± SEM. Statistical significance was determined by *t* test. ###, $P < 0.001$; ##, $P < 0.01$; #, $P < 0.05$.

We next evaluated the role of MC2R during prolonged starvation. After 36 h of starvation, liver gluconeogenesis becomes the major source of blood glucose (14). During a 36-h fast, MC2R KO mice exhibited a faster decline in blood glucose levels (Fig. 6*A*): male $MC2R^{-/-}$, 45.8 ± 11.7 mg/dl ($n = 5$); and $MC2R^{+/+}$, 79.2 ± 9.5 mg/dl ($n = 5$). As anticipated, corticosterone levels in WT mice were increased in response to fasting, whereas corticosterone levels in MC2R KO mice were not increased in response to a 36-h fast (Fig. 6*B*): male $MC2R^{-/-}$, undetectable ($n = 5$); and $MC2R^{+/+}$, 94.4 ± 23.4 ng/ml ($n = 5$). Serum epinephrine was significantly decreased in MC2R KO mice, whereas norepinephrine, dopamine, insulin, and glucagon levels (data not shown) were not significantly different. The expression of PEPCK, which is a rate-limiting enzyme in gluconeogenesis, was significantly decreased, and G6Pase was relatively decreased in MC2R KO mice after a prolonged (36 h) fast (Fig. 6*C*), indicating that the lower blood glucose levels in MC2R KO mice were due to impaired gluconeogenesis.

Discussion

Immediately after birth, the maternal supply of substrates ceases abruptly, and the newborn mouse has to withstand a brief period of starvation before being fed with milk that is high in fat and low in carbohydrates. The adaptation of neonates to these changes in nutrition and environment requires modification of glucose and fatty acid metabolism, which is controlled by the neonatal increase in glucagon and the fall in insulin (15). Defective gluconeogenesis leads to neonatal death (16). Plasma corticosterone levels are high at delivery and rapidly decline during the first 24 h after birth, and epinephrine and norepinephrine levels are increased severalfold in newborns in response to the stresses of birth, such as transient hypoxia, cold exposure, and cord cutting (15). Because GC plays a critical role in the maintenance of neonatal blood glucose levels through the induction of

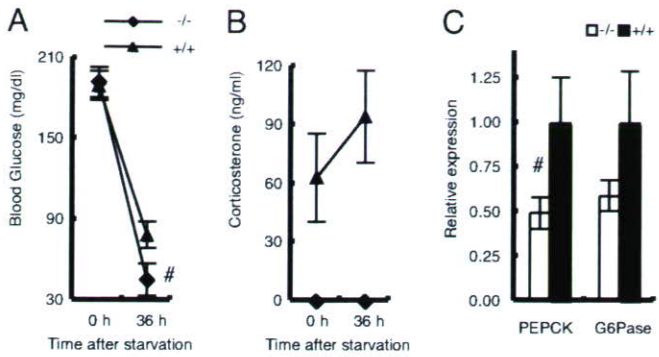

Fig. 6. MC2R KO mice develop hypoglycemia during fasting. The experiment was performed with 12-wk-old male $MC2R^{-/-}$ ($n = 5$) and $MC2R^{+/+}$ ($n = 5$) mice. (*A* and *B*) At time 0 (2000 hours), food was withdrawn and blood glucose (*A*) and serum corticosterone level (*B*) were measured. After 36 h, mice (at 0800 hours) were killed and serum samples and liver RNA were prepared. Expression of phosphoenolpyruvate carboxykinase (PEPCK) and glucose-6-phosphatase (G6Pase) in the liver was determined by qRT-PCR (*C*). Data are expressed as means ± SEM. The statistical difference was evaluated by two-way ANOVA (factor 1 was genotype and factor 2 was treatment) followed by *t* test to compare the significant difference between the glucose value for 36 h of MC2R KO mice and the glucose value for 36 h of WT mice. #, $P < 0.05$.

gluconeogenesis, one-half of hepatocyte-specific GC receptor KO mice die shortly after birth as a result of hypoglycemia (17). Here, we demonstrated that MC2R KO mice are defective in this adaptation, consistent with a previous report that 75% of POMC KO mice die shortly after birth (2). Genetic replacement of pituitary POMC in POMC KO mice ($POMC^{-/-}Tg^{+}$) rescues neonatal lethality in POMC KO mice, suggesting that peripheral POMC, possibly ACTH, is important for neonatal survival (18). These results collectively suggest that ACTH MC2R signaling plays a critical role in the neonatal adaptation to nutrition supply, consistent with the fact that patients with FGD often suffer from neonatal hypoglycemia (OMIM no. 202200) (19). Neonatal hypoglycemia in MC2R KO mice might be secondary to low levels of both circulating corticosterone and epinephrine. It is also interesting that a slight increase in mortality was also observed at 3–4 wk of age because weaning is a crucial period when mice need to adapt to nutritional modifications. In fact, corticosterone concentration is low during the suckling period, increases after 12 days, and peaks at 24 days (15). Further studies are required to clarify the possible role of ACTH MC2R in suckling/weaning adaptation.

We observed significant adrenocortical hypoplasia in adult MC2R KO mice compared with WT siblings. Although zG cells remained fairly intact, zF cells were severely atrophied (Fig. 2), indicating that MC2R is not required for proper development of zG cells but is required for that of zF cells. Adrenal glands of rodents possess a transient zone between the adrenal cortex and the adrenal ME called the murine X zone. The overall function of the X zone remains unclear (20). Detailed studies are required to clarify the possible effect of ACTH deficiency on X zone regression. Because the adrenal glands from MC2R KO pups were indistinguishable in size and histological appearance from those from WT littermates at birth (data not shown), consistent with POMC KO mice (21), the ACTH MC2R signaling pathway regulates postnatal development of the adrenal gland. It was previously proposed that POMC-derived peptides other than ACTH contribute to adrenal development, function, and maintenance. Specifically, cleavage of the N-terminal POMC (amino acids 1–74) results in the generation of shorter peptides with mitogenic properties (22). If POMC-derived peptides other than ACTH have any role in adrenal development, the adrenal phenotype of MC2R KO mice should be less severe than that of POMC KO mice. Compared with the adrenal structure of POMC KO mice previously reported (2, 4), the adrenal structure/morphology of MC2R KO mice was intact, especially in zG. The total number of nuclei in zF of MC2R KO mice was not significantly changed (Fig. 2*A*), suggesting that the proliferation of zF in MC2R KO mice was comparable with that in WT mice. In contrast, it was previously demonstrated that adrenal glands of POMC KO mice on postnatal day 14 had reduced proliferating cell nuclear antigen (PCNA)-positive cells (21). These differences could be explained by the possible role of POMC-derived peptides other than ACTH in adrenal development (22), although we could not exclude the possibility of difference due to genetic background or of compensatory function by other MCRs in the absence of MC2R. Simultaneous comparison of POMC KO mice and MC2R KO mice is required to clarify these possibilities.

We analyzed the adrenal gene expression involved in the syntheses of corticosterone, aldosterone, and catecholamines in MC2R KO mice at 12 wk of age. Two previous studies have shown adrenal gene expression profiles in POMC KO mice. Karpac *et al.* (21) demonstrated that the expression of Cyp11b2, Cyp11b1, and TH in POMC KO mice at 5 wk of age was not significantly different from that in WT mice and suggested that the essential role for POMC peptides is in the maintenance of the adrenal gland and not in differentiation. Coll *et al.* (23) also analyzed the expression of Cyp11b1 and Cyp11a1 and demonstrated that the expression of both was reduced in POMC KO mice at 8 wk of age. Although the latter results were consistent with ours, the former results were not. We could not fully explain the reason for the difference: however, one possible explanation is that adrenal glands of POMC KO and MC2R KO mice at 5 wk of age are indistinguishable from those of WT mice and that they regress thereafter, as suggested by Karpac *et al.* (21). Further developmental studies on the adrenal gland in POMC KO and MC2R KO mice are needed to clarify these issues.

We found that the adrenal glands in MC2R KO mice produce aldosterone at reduced levels, as has been observed in POMC KO mice (2, 4). In this regard, the MC2R-deficient mouse model is different from FGD type 1 patients, who have been reported to exhibit normal serum aldosterone levels (24). This disparity could be explained by the fact that the majority of humans have one or two missense alleles, and homozygous nonsense mutations are very rare. It was recently reported that a small number of such patients may provide biochemical evidence of mineralocorticoid deficiency (25). The role of ACTH in aldosterone production is further supported by the fact that glucocorticoid receptor (GR) KO mice had enlarged adrenal glands with greatly increased expression of not only Cyp11b1 but also Cyp11b2 at embryonic day 18.5 (26). GR KO mice had increased ACTH levels as a result of the deficiency of negative feedback by corticosterone (26). It is possible that increased ACTH levels in GR KO mice are directly responsible for the increased expression of Cyp11b2 in zG. These observations collectively indicate that ACTH MC2R signaling is an important regulator of aldosterone production.

Here we described the initial characterization of MC2R KO mice and confirmed and extended the importance of ACTH-MC2R in neonatal adaptation to nutrition supplies, adrenal development, and the production of corticosterone and aldosterone. The possible role of ACTH-MC2R in adipose metabolism (27), β-cell function (28), and skin homeostasis (29) could be clarified by further analysis of MC2R KO mice.

Materials and Methods

Animals. Generation of MC2R KO mice is described in *SI Materials and Methods*. For analysis of tissue weight, 12-wk-old mice of each genotype were evaluated. Adrenal glands were dissected, cleaned of fat under a stereoscopic microscope, and

weighed. Epididymal white adipose tissue, inguinal white adipose tissue, thymus, and spleen were dissected and weighed. Whole-tissue samples were isolated and placed on saline-saturated filter papers to remain hydrated until weighing. All of the mice were kept under specific pathogen-free conditions in an environmentally controlled clean room in the Laboratory Animal Research Center, Institute of Medical Science, University of Tokyo. The experiments were conducted according to institutional ethical guidelines for animal experiments and safety guidelines for gene manipulation experiments.

Blood Analysis. For analysis of basal hormone levels, 12-wk-old adult mice of each genotype were evaluated. After 8 h of fasting, at 1600 hours, mice were anesthetized with diethyl ether, and blood samples were collected rapidly from the heart. Serum electrolyte concentrations were measured by the ion-selective electrode method (SRL, Tokyo, Japan). Serum corticosterone, ACTH, and aldosterone levels were determined by RIA with detection limits of 4.8 ng/ml (Amersham, Little Chalfont, United Kingdom), 5 pg/ml (Mitsubishi, Tokyo, Japan), and 0.05 ng/ml (Aldosterone-RIAKIT II; SRL), respectively. Serum catecholamine levels were determined by HPLC (SRL). Male $MC2R^{+/+}$, $MC2R^{+/-}$, and $MC2R^{-/-}$ mice of 12 wk of age were injected i.p. at 1000 hours with either ACTH (Peptide Institute, Osaka, Japan) at a dose of 10 μg/kg or saline. Animals were killed by decapitation, and blood was collected after 60 min.

Blood Pressure Measurement. Blood pressure and heart rate were measured in conscious mice by the indirect tail-cuff method (BP-98A; Softron, Tokyo, Japan) as described in ref. 30.

Histology and qRT-PCR Analysis. Histochemical procedures are described in *SI Materials and Methods*. For determination of relative mRNA concentrations, total adrenal gland or liver RNA, isolated by sepazol, was subjected to reverse transcription by using SuperScript III (Invitrogen, Carlsbad, CA). The cDNA was analyzed by automated fluorescent real-time PCR with SYBR Green (Invitrogen) by using an iCycler iQ (Bio-Rad, Hercules, CA). Ribosomal protein S3 (RPS3) was used as a control. Primer sequences were designed by using Universal ProbeLibrary Assay Design Center (www.roche-applied-science.com/sis/rtpcr/upl/adc.jsp) (Roche Applied Science, Indianapolis, IN) or Primer Bank (http://pga.mgh.harvard.edu/primerbank) (31) as described in *SI Materials and Methods*.

Statistical Analysis. All values were calculated as means ± SEM. Comparisons of two groups were analyzed by using Student's t test; for comparisons of more than two groups, one- or two-way ANOVA was performed, followed by Fisher's protected least significant difference (PLSD) tests, to analyze statistical differences in each group. In all analyses, a two-tailed probability of $<5\%$ (i.e., $P < 0.05$) was considered statistically significant.

We thank all of the members of our laboratory for discussion and help with animal care; Dr. Michael S. Patrick for critical reading of this manuscript; and Dr. Atsushi Miyajima (University of Tokyo), Dr. Hiroshi Takemori (National Institute of Biomedical Innovation, Osaka, Japan), and Kuniaki Mukai (Keio University) for reagents. We express our condolences on Dr. Kubo's sudden death during the preparation of this manuscript. This work was supported by grants from the Ministry of Education, Culture, Sports, Science, and Technology of Japan and the Ministry of Health, Labor, and Welfare of Japan.

1. Dallman MF (1984) *Endocr Res* 10:213–242.
2. Yaswen L, Diehl N, Brennan MB, Hochgeschwender U (1999) *Nat Med* 5:1066–1070.
3. Challis BG, Coll AP, Yeo GS, Pinnock SB, Dickson SL, Thresher RR, Dixon J, Zahn D, Rochford JJ, White A, *et al.* (2004) *Proc Natl Acad Sci USA* 101:4695–4700.
4. Coll AP, Challis BG, Yeo GS, Snell K, Piper SJ, Halsall D, Thresher RR, O'Rahilly S (2004) *Endocrinology* 145:4721–4727.
5. Smart JL, Tolle V, Otero-Corchon V, Low MJ (2007) *Endocrinology* 148:647–659.
6. Clark AJL, Weber A (1998) *Endocr Rev* 19:828–843.
7. Metherell LA, Chapple JP, Cooray S, David A, Becker C, Ruschendorf F, Naville D, Begeot M, Khoo B, Nurnberg P, *et al.* (2005) *Nat Genet* 37:166–170.
8. Genin E, Huebner A, Jaillard C, Faure A, Halaby G, Saka N, Clark AJ, Durand P, Begeot M, Naville D (2002) *Hum Genet* 111:428–434.
9. Shimizu C, Kubo M, Saeki T, Matsumura T, Ishizuka T, Kijima H, Kakinuma M, Koike T (1997) *Gene* 188:17–21.
10. Clark AJ, Cammas FM, Watt A, Kapas S, Weber A (1997) *J Mol Med* 75:394–399.
11. Coll AP, Challis BG, Lopez M, Piper S, Yeo GS, O'Rahilly S (2005) *Diabetes* 54:2269–2276.
12. Miller WL (1988) *Endocr Rev* 9:295–318.
13. Finotto S, Krieglstein K, Schober A, Deimling F, Lindner K, Bruhl B, Beier K, Metz J, Garcia-Arraras JE, Roig-Lopez JL, *et al.* (1999) *Development (Cambridge, UK)* 126:2935–2944.
14. Pilkis SJ, Granner DK (1992) *Annu Rev Physiol* 54:885–909.
15. Girard J, Ferre P, Pegorier JP, Duee PH (1992) *Physiol Rev* 72:507–562.
16. Wang ND, Finegold MJ, Bradley A, Ou CN, Abdelsayed SV, Wilde MD, Taylor LR, Wilson DR, Darlington GJ (1995) *Science* 269:1108–1112.
17. Tronche F, Opherk C, Moriggl R, Kellendonk C, Reimann A, Schwake L, Reichardt HM, Stangl K, Gau D, Hoeflich A, *et al.* (2004) *Genes Dev* 18:492–497.
18. Smart JL, Tolle V, Low MJ (2006) *J Clin Invest* 116:495–505.
19. Clark AJ, Metherell LA, Cheetham ME, Huebner A (2005) *Trends Endocrinol Metab* 16:451–457.
20. Hershkovitz L, Beuschlein F, Klammer S, Krup M, Weinstein Y (2007) *Endocrinology* 148:976–988.
21. Karpac J, Ostwald D, Bui S, Hunnewell P, Shankar M, Hochgeschwender U (2005) *Endocrinology* 146:2555–2562.
22. Estivariz FE, Iturriza F, McLean C, Hope J, Lowry PJ (1982) *Nature* 297:419–422.
23. Coll AP, Fassnacht M, Klammer S, Hahner S, Schulte DM, Piper S, Tung YC, Challis BG, Weinstein Y, Allolio B, *et al.* (2006) *J Endocrinol* 190:515–525.
24. Clark AJ, McLoughlin L, Grossman A (1993) *Lancet* 341:461–462.
25. Lin L, Hindmarsh PC, Metherell LA, Alzyoud M, Al-Ali M, Brain CE, Clark AJ, Dattani MT, Achermann JC (2007) *Clin Endocrinol (Oxford)* 66:205–210.
26. Cole TJ, Blendy JA, Monaghan AP, Krieglstein K, Schmid W, Aguzzi A, Fantuzzi G, Hummler E, Unsicker K, Schutz G (1995) *Genes Dev* 9:1608–1621.
27. Boston BA, Cone RD (1996) *Endocrinology* 137:2043–2050.
28. Genuth S, Lebovitz HE (1965) *Endocrinology* 76:1093–1099.
29. Arck PC, Slominski A, Theoharides TC, Peters EM, Paus R (2006) *J Invest Dermatol* 126:1697–1704.
30. Matsuki T, Isoda K, Horai R, Nakajima A, Aizawa Y, Suzuki K, Ohsuzu F, Iwakura Y (2005) *Circulation* 112:1323–1331.
31. Wang X, Seed B (December 15, 2003) *Nucleic Acids Res* 31, 10.1093/nar/gng154.

J Neuropathol Exp Neurol

Vol. 66, No. 11
November 2007
pp. 1037–1044

ORIGINAL ARTICLE

Intrathecal Delivery of Hepatocyte Growth Factor From Amyotrophic Lateral Sclerosis Onset Suppresses Disease Progression in Rat Amyotrophic Lateral Sclerosis Model

Aya Ishigaki, MD, PhD, Masashi Aoki, MD, PhD, Makiko Nagai, MD, PhD, Hitoshi Warita, MD, PhD, Shinsuke Kato, MD, PhD, Masako Kato, MD, PhD, Toshikazu Nakamura, PhD, Hiroshi Funakoshi, MD, PhD, and Yasuto Itoyama, MD, PhD

Abstract

Hepatocyte growth factor (HGF) is one of the most potent survival-promoting factors for motor neurons. We showed that introduction of the HGF gene into neurons of G93A transgenic mice attenuates motor neuron degeneration and increases the lifespan of these mice. Currently, treatment regimens using recombinant protein are closer to clinical application than gene therapy. To examine its protective effect on motor neurons and therapeutic potential we administered human recombinant HGF (hrHGF) by continuous intrathecal delivery to G93A transgenic rats at doses of 40 or 200 μg and 200 μg at 100 days of age (the age at which pathologic changes of the spinal cord appear, but animals show no clinical weakness) and at 115 days (onset of paralysis), respectively, for 4 weeks each. Intrathecal administration of hrHGF attenuates motor neuron degeneration and prolonged the duration of the disease by 63%, even with administration from the onset of paralysis. Our results indicated the therapeutic efficacy of continuous intrathecal administration of hrHGF in transgenic rats and should lead to the consideration for further clinical trials in amyotrophic lateral sclerosis using continuous intrathecal administration of hrHGF.

Key Words: Amyotrophic lateral sclerosis, Continuous intrathecal delivery, Hepatocyte growth factor, Neurodegeneration, Superoxide dismutase-1 (SOD1), Transgenic rat.

From the Department of Neurology (AI, MA, MN, HW, YI), Tohoku University Graduate School of Medicine, Sendai, Japan; Tohoku University Hospital ALS Center (AI, MA, HW, YI), Sendai, Japan; Department of Neuropathology (SK), Institute of Neurological Sciences, Faculty of Medicine Tottori University, Yonago, Japan; Division of Pathology (MK), Tottori University Hospital, Yonago, Japan; and Division of Molecular Regenerative Medicine (TN, HF), Department of Biochemistry and Molecular Biology, Osaka University Graduate School of Medicine, Osaka, Japan.

Send correspondence and reprint requests to: Masashi Aoki, MD, PhD, Department of Neurology, Tohoku University Graduate School of Medicine, 1-1 Seiryo-machi, Sendai 980-8574, Japan; E-mail: aokim@mail.tains.tohoku.ac.jp

This work was supported by a grant from the Ministry of Health, Labor, and Welfare, Japan (YI, MA, SK, HF). Research funding was also provided by the Haruki ALS Research Foundation (YI, MA, HW) and by a Grant-in-Aid for Scientific Research from the Ministry of Education, Culture, Sports, Science, and Technology, Japan (MA, SK, HF).

INTRODUCTION

Amyotrophic lateral sclerosis (ALS) is a fatal neurodegenerative disease caused by selective motor neuron death (1). Approximately 10% of cases of ALS are inherited, usually as an autosomal dominant trait (2). In ~25% of familial cases, the disease is caused by mutations in the gene encoding cytosolic copper-zinc superoxide dismutase (SOD1) (3–5). The cause of ALS is still unclear, and clinical trials have as yet failed to identify any truly effective therapeutic regimens for ALS, with only riluzole providing a modest improvement in survival. Various substances have been shown to have therapeutic effects in a murine model of ALS. However, there have been a few reports of prolongation of survival with treatment starting around the time of disease onset (6–12).

We (13) and another group (14) developed a rat model of ALS expressing a human SOD1 transgene with 2 ALS-associated mutations: glycine to alanine at position 93 (G93A) and histidine to arginine at position 46 (H46R) (3, 5). Similar to its murine counterpart, this rat transgenic (Tg) ALS model reproduces the major phenotypic features of human ALS. Some experimental manipulations are difficult in Tg mice because of size limitations; however, this Tg rat model allows routine implantation of infusion pumps for intrathecal drug delivery. Intrathecal drug application is a well-established method for therapy and has been used in clinical trials in patients with ALS (15). This route of administration bypasses the blood-brain barrier, allowing rapid access to potential binding sites for the test compound in the spinal cord (16).

Hepatocyte growth factor (HGF) was first identified as a potent mitogen for mature hepatocytes and was first cloned in 1989 (17). Detailed studies indicated that HGF is expressed in the CNS (18) and is a novel neurotrophic factor (19, 20). HGF is one of the most potent survival-promoting factors for motor neurons, comparable to glial cell line-derived neurotrophic factor in vitro (21). Sun et al (22) reported that introduction of the HGF gene into neurons of G93A Tg mice attenuates motor neuron degeneration and increases the lifespan of these mice. Thus, HGF is a good candidate agent for treatment of ALS. Currently, treatment using recombinant protein is closer to clinical application than gene therapy. However, HGF has a very

short half-life (23–25) and shows poor penetration into the CNS. Therefore, we examined the effects of continuous intrathecal delivery of human recombinant HGF (hrHGF) into Tg rats using implanted infusion pumps for selective and less invasive supply of HGF to the spinal cord.

MATERIALS AND METHODS

Animal Preparation and Clinical Evaluation

G93A Tg rats were genotyped by polymerase chain reaction (PCR) assay using DNA obtained from the tail as described (13). To examine the dose and effects of hrHGF on disease onset, we began administration of 40 or 200 μg of hrHGF (provided by H. Funakoshi and T. Nakamura, Osaka University, Osaka, Japan) or vehicle (0.1 M sulfoxide PBS) for 4 weeks to groups of eight 100-day-old Tg rats, when the pathologic changes of the spinal cord appeared, but the animals did not show weakness. All animals were killed at 130 days by deep anesthesia, and the spinal cords were examined. Because treatment of patients with ALS patients is initiated only after diagnosis based on clinical signs and symptoms, we tested the effects of hrHGF on survival with administration beginning at around the age of onset of paralysis. We administered 200 μg of hrHGF or vehicle alone to groups of eight 115-day-old G93A Tg rats for 4 weeks, and the animals were observed until their death. To analyze the mechanism of action of hrHGF administration beginning at onset of paralysis we treated groups of six 115-day-old G93A Tg rats with 100 μg of hrHGF or with vehicle alone for 2 weeks (a dose comparable to 200 μg for 4 weeks). All rats were killed 2 weeks after commencement of administration of hrHGF, and their lumbar spinal cords were examined. Further groups of 3 G93A Tg rats and 3 non-Tg rats at 70, 100, and 130 days were used to measure the levels of rat HGF and c-Met. All rats were handled according to approved animal protocols of our institution and had free access to food and water throughout the experimental period and before and after pump implantation.

The onset of ALS was scored as the first observation of abnormal gait, evidence of limb weakness, or loss of extension of the hindlimbs when picked up at the base of the tail. We defined the appearance of paralysis as disease onset, although this is not a sensitive indicator and appears later than the decrease in activity (10). However, the appearance of paralysis is a suitable marker of disease onset because it is closer to the state at which patients will be diagnosed with the disease.

Footprints were collected every 3 days by letting the rats walk on a straight path after dipping their hind paws in black ink. We measured 3 strides within the area showing regular gait and calculated the means. Footprint measurements were made for rats that began treatment at 115 days. Examiners were blinded to which group each of the rats belonged in.

Preparation of the Osmotic Pumps and Transplant Surgery

Osmotic pumps (model number 2004 or 2002; Durect Corporation, Cupertino, CA) were incubated in sterile saline at 37°C for 40 hours to attain a constant flow rate before use. Pumps were filled to capacity with hrHGF solution or vehicle using a filling needle. An infusion tube was made by connecting a 1-cm length of polyethylene tubing (PE 60; Becton Dickinson, Franklin Lakes, NJ) to a small caliber tube 9 cm in length (PE 10; Becton Dickinson) using an adhesive (ARON ALPHA; Konishi Co., Osaka, Japan). The end of the infusion tube was connected to the shorter end of the flow moderator, the longer end of which was inserted into the pump.

Surgery for placement of the pump and intrathecal administration was performed as follows. Tg rats were anesthetized using diethyl ether and 1% halothane in a mixture of 30% oxygen and 70% nitrous oxide. The skin over the third to fifth lumbar spinal process was incised and the paravertebral muscles were separated from the vertebral lamina with scissors. The fifth lumbar vertebra was laminectomized, and the dura mater was exposed for insertion of the infusion tube. Particular care was taken not

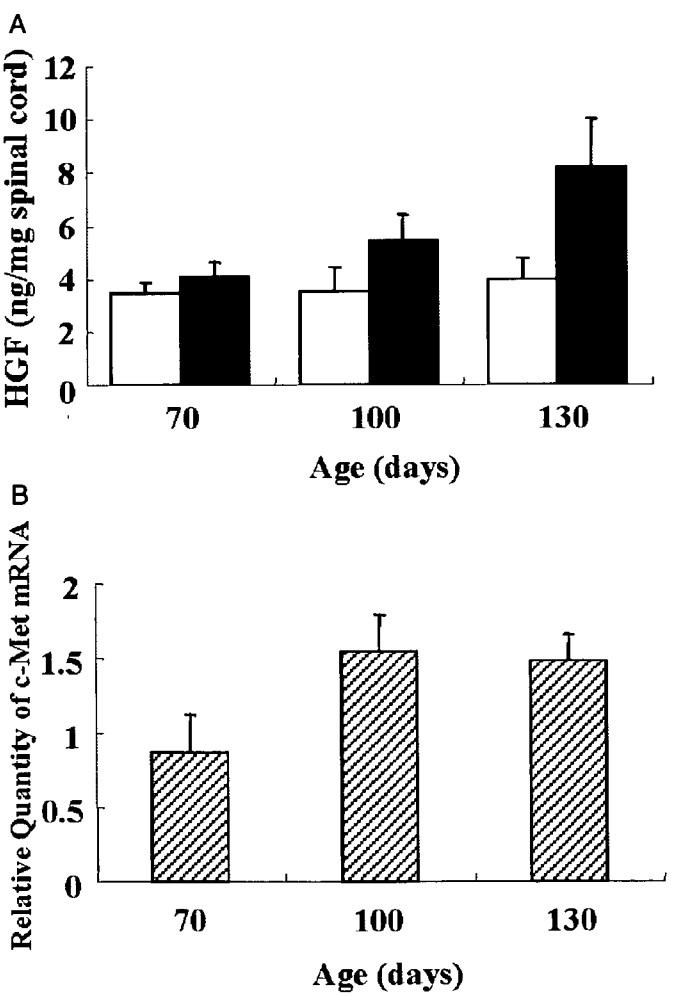

FIGURE 1. Increased levels of rat hepatocyte growth factor (HGF) and c-Met expression in the spinal cords of G93A transgenic (Tg) rats (n = 3) and non-Tg rats (n = 3). **(A)** Levels of endogenous rat HGF expression. Open bars, non-Tg rats; closed bars, G93A Tg rats. **(B)** Levels of c-Met mRNA of G93A Tg rats compared with non-Tg rats.

to injure the dura mater during laminectomy. A small hole was bored through the dura mater with a 24-gauge needle, and a polyethylene tube (PE 10, Becton Dickinson) was inserted into the subarachnoid space approximately 3 cm rostrally. A subcutaneous pocket was made into which the osmotic pump and pump side tube were implanted. The infusion tube was attached to the fascia over the paravertebral muscles at the incision margin with silk string. A drop of adhesive (ARON ALPHA) was applied, and the incision was closed by suturing the muscles and skin.

Measurement of Rat and Human HGF in the Lumbar Spinal Cord

Slices of the fifth lumbar cord from 3 G93A Tg rats and 3 non-Tg rats at 70, 100, and 130 days as well as from 130-day-old G93A Tg rats treated with 40 or 200 μg of hrHGF or vehicle alone for 4 weeks starting at 100 days were homogenized in buffer (20 mM Tris-HCl, pH 7.5, 0.1% Tween-80, 1 mM phenylmethylsulfonyl fluoride, and 1 mM EDTA) and centrifuged at 15,000 rpm for 30 minutes. Supernatants were separated and the concentrations of rat endogenous HGF were measured using an enzyme-linked immunosorbent assay (ELISA) kit, which is specific for rat HGF without detecting human HGF (22) (Institute of Immunology, Tokyo, Japan). For measurement of human HGF in the treated rats we used a human HGF-specific ELISA kit (IMMUNIS, Institute of Immunology), which is not reactive with rat HGF (26, 27).

Measurement of c-Met mRNA in the Lumbar Spinal Cord of Tg Rats

Aliquots of 1 μg of total RNA from the lumbar cords of rats were used as templates for synthesis of double-stranded cDNA. Real-time quantitative PCR was performed for c-Met and glyceraldehyde-3-phosphate dehydrogenase (GAPDH) [GAPDH forward primer, 5′-CCATCACTGCCACTCAGAAGAC-3′; GAPDH reverse primer, 5′-TCATACTTGGCAGGTTTCTCCA-3′; GAPDH TaqMan probe, 5′(FAM)-ACCACGAGCACTGTTTCAATAGGACCC-(TAMRA)3′; c-MET forward primer, 5′-GTACGGTGTCTCCAGCATTTTT-3′; c-Met reverse primer, 5′-AGAGCACCACCTGCATGAAG-3′; TaqMan probe, 5′(FAM)-CGTGTTCCTACCCCCAATGTATCCGT- (TAMRA)3′]. An ABI Prism 7700 Sequence Detection System (Applied Biosystems Perkin-Elmer, Foster City, CA) was used to monitor emission intensities using the above primer pairs and TaqMan fluorogenic probes. The c-Met mRNA level of G93A Tg rats relative to non-Tg rats was calculated using the Comparative C_T Method (Applied Biosystems).

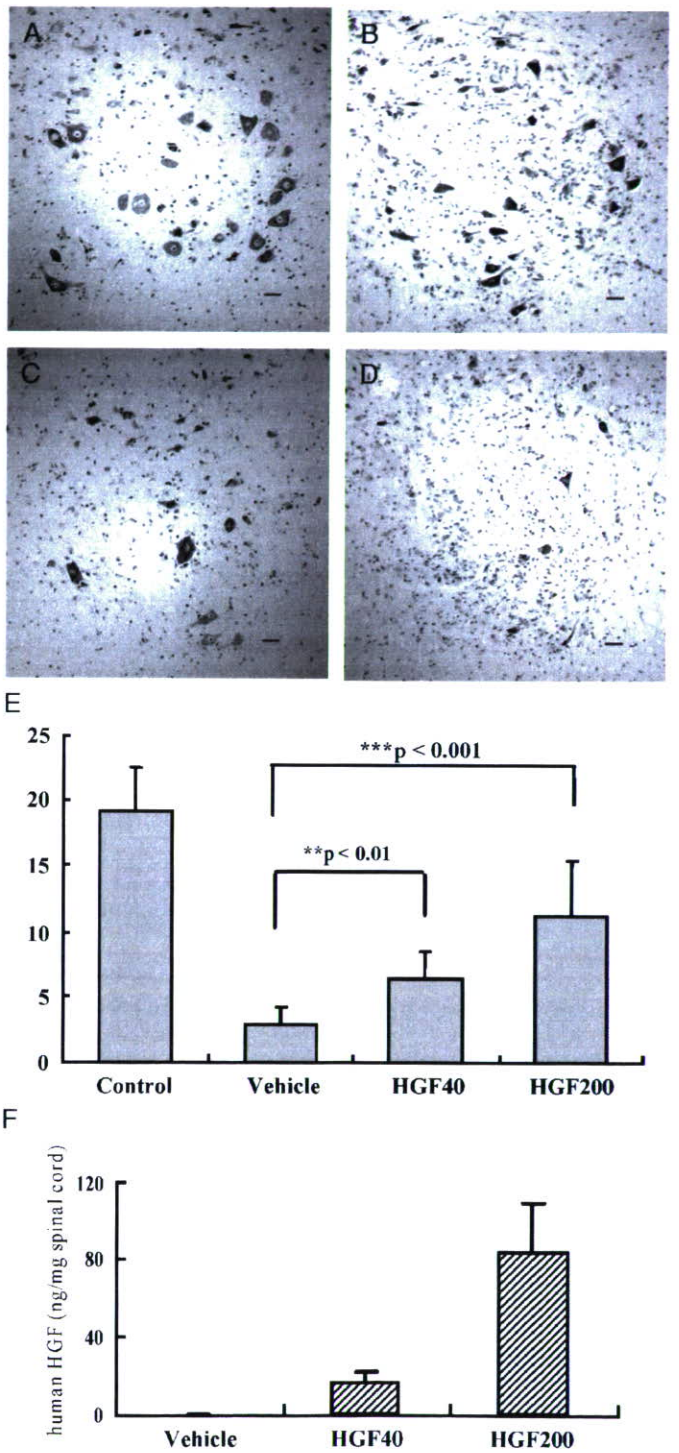

FIGURE 2. Intrathecal administration of hepatocyte growth factor (HGF) to G93A transgenic (Tg) rats at 100 days showed a protective effect against motor neuron death. **(A–D)** Histologic evaluation of the anterior horn with Nissl staining at 130 days: **(A)** lumbar cord of non-Tg rats; **(B)** 200 μg of human recombinant HGF (hrHGF)-treated; **(C)** 40 μg of hrHGF-treated; and **(D)** vehicle-treated G93A Tg rats. Scale bar = 40 μm. **(E)** Quantitative morphometric evaluation of surviving motor neurons of the fifth lumbar anterior horn at 130 days. We counted neurons that were >40 μm in diameter. Significantly larger numbers of motor neurons survived in hrHGF-treated G93A Tg rats ($p < 0.01$ and $p < 0.001$, 40 and 200 μg of hrHGF, respectively), compared with vehicle-treated G93A Tg rats ($n = 8$ in each group). **(F)** Levels of human HGF concentration in lumbar spinal cords of G93A Tg rats treated with 200 μg of hrHGF, 40 μg of hrHGF, and vehicle.

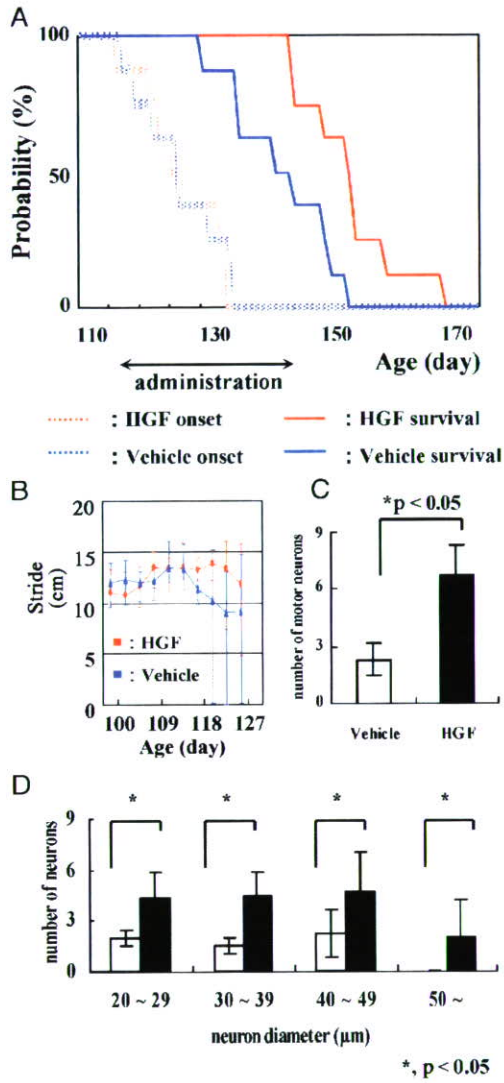

FIGURE 3. Intrathecal administration of hepatocyte growth factor (HGF) from 115 days (just before disease onset) retarded disease progression. **(A)** Survival periods were 143.25 ± 17.0 days in the vehicle-treated group (solid blue line) and 154.3 ± 16.4 days in the 200 μg of human recombinant HGF (hrHGF)-treated group (solid red line). Survival of hrHGF-treated animals was extended significantly ($p = 0.0135$), although there were no significant differences in onset (dotted lines, $n = 8$ in each group, $p = 0.6346$). **(B)** Footprint analysis demonstrated a delay in decline of stride length in G93A transgenic (Tg) rats treated with 200 μg of hrHGF relative to vehicle-treated G93A Tg rats (error bars, ± SD). **(C, D)** Quantitative morphometric evaluation of surviving motor neurons that were >40 μm in diameter **(C)** and neuron size distribution **(D)** in the fifth lumbar anterior horn of G93A Tg rats 2 weeks after administration from 115 days. Significantly larger number of motor neurons survived in the hrHGF-treated G93A Tg rats compared with vehicle-treated G93A Tg rats (6.7 ± 1.6 vs 2.3 ± 0.9; $p = 0.002$, $n = 6$ in each group) **(C)**.

Histopathologic and Immunohistochemical Analyses

To examine the dose and effects of hrHGF against disease onset, we began administration of 40 or 200 μg of hrHGF or vehicle alone to groups of eight 100-day-old Tg rats each for 4 weeks. At 130 days, G93A Tg rats were administered hrHGF or vehicle, and non-Tg rats were deeply anesthetized with diethyl ether and killed for histopathologic evaluation. To examine the effects of hrHGF administration beginning at onset of paralysis, 100 μg of HGF or vehicle alone was administered to groups of six 115-day-old Tg rats for 2 weeks. These animals were killed by deep anesthesia with diethyl ether 2 weeks after the operation. Under deep anesthesia these animals were perfused via the aorta with physiologic saline at 37°C and their lumbar spinal cords were removed. The fifth lumbar spinal cord tissue was embedded in OCT compound (Sakura Finetek Japan Co., Tokyo, Japan), frozen in an acetone/dry ice bath after fixation with 4% paraformaldehyde, and supplemented with 0.1 M cacodylate buffer (pH 7.3) containing 30% sucrose. Other spinal cord tissue specimens were frozen in dry ice and cut into frozen sections (12-μm-thick) and then washed with PBS. To evaluate the effects of HGF on motor neuron loss we compared the numbers of lumbar motor neurons in each group by counting as mentioned below. To evaluate the effects of HGF on apoptosis and to determine whether HGF receptors were activated, we compared the results of immunohistochemical staining of the lumbar cords for activated caspase-3, activated caspase-9 (Cell Signaling Technology, Inc., Beverly, MA), and phosphorylated c-Met (activated HGF receptor) (BioSource International, Camerillo, CA). The staining specificity of the antibodies was assessed by preabsorption of the primary antibody with excess peptide, omission of the primary antibody, or replacement of the primary antibody with normal rabbit IgG (22). We examined every seventh section from 42 serial sections of the fifth lumbar spinal cord. We counted neurons that had a clear nucleolus and were multipolar with neuronal morphology (13, 22), >40 μm in diameter, and located in a defined area of the anterior horn of the spinal cord. Cell counts were performed using ImageJ software (National Institutes of Health, Bethesda, MD) on images captured electronically (28).

Western Blotting

Lysates from the lumbar spinal cord of each rat were prepared in RIPA buffer (150 mM NaCl, 1% Nonidet P-40, 0.5% deoxycholate, 0.1% sodium dodecyl sulfate, and 50 mM Tris, pH 8.0). Equal amounts of proteins from the lysates (50 μg) were resolved by sodium dodecyl sulfate-polyacrylamide gel electrophoresis, transferred onto polyvinylidene diflouride membranes, and immunoblotted. The primary antibodies used were anti-caspase-3 (Sigma-Aldrich, St. Louis, MO), anti-caspase-9 (Stressgen Biotechnologies Corporation, Victoria, BC, Canada), anti-X-linked inhibitor of apoptosis protein (XIAP) (Cell Signaling Technology, Inc.), and anti-excitatory amino acid transporter 2 (EAAT2) antibodies (Chemicon International, Temecula, CA). After incubation of membranes with HRP-coupled

secondary antibodies, proteins were visualized using ECL or ECL Plus Western Blotting Detection Reagents (Amersham Biosciences Inc., Piscataway, NJ) and a Fluorochem image analyzer (LAS-3000 mini; Fuji Photo Film Co., Tokyo, Japan).

Statistical Analysis

The Kaplan-Meier and log-rank test were used for statistical analyses of differences in onset and survival between groups. For statistical analyses of differences in body weight, footprint, motor neuron cell count, and Western blotting we used analysis of variance and post hoc tests. The data are reported as means ± SD.

RESULTS

Measurement of the Levels of Rat HGF and c-Met Expression in Untreated Animals

Groups of 3 G93A Tg rats and non-Tg rats at 70, 100, and 130 days were used to measure the levels of rat HGF without any treatment. In the lumbar cords of untreated G93A Tg rats, the HGF concentrations increased with disease progression (Fig. 1A). At 70 days the level of rat HGF in the lumbar cords of G93A Tg rats was 4.05 ± 0.6 ng/mg and was the same as that of non-Tg rats. Increases of 35% and 107% were observed in the rat HGF level at 100 and 130 days, respectively, compared with non-Tg rats.

In addition, we measured the levels of c-Met mRNA in the lumbar spinal cords of Tg rats relative to non-Tg rats by real-time quantitative PCR. In the lumbar cords of G93A Tg rats the level of c-Met mRNA expression was the same as that in non-Tg rats at 70 days. However, a 55% increase in the level of c-Met mRNA expression compared with that of non-Tg rats was observed at 100 days and the higher level of expression was retained at 130 days (Fig. 1B).

Administration of hrHGF to 100-Day-Old G93A Tg Rats for 4 Weeks

To examine the efficacy of hrHGF on motor neurons in the spinal cords of Tg rats against onset of disease we administered 40 and 200 μg of hrHGF or vehicle alone to 100-day-old G93A Tg rats for 4 weeks (n = 8 in each group). Animals were killed at 130 days, and their lumbar spinal cords were examined. Because administration of hrHGF for more than 30 days may induce antibodies against hrHGF, we did not treat rats for longer than this period. We confirmed elevation of human HGF concentrations in the lumbar cords of hrHGF-treated rats using a specific sandwich immunoassay. The mean human HGF concentrations were 83.9 ± 25.1, 15.6 ± 5.4, and 0 ng/mg for rats treated with 200 μg of hrHGF, 40 μg of hrHGF, and vehicle, respectively (Fig. 2F). The endogenous rat HGF concentration is 4 to 5 ng/mg at this age (Fig. 1A). The human HGF concentration in the spinal cord of G93A Tg rats treated with 200 μg of hrHGF

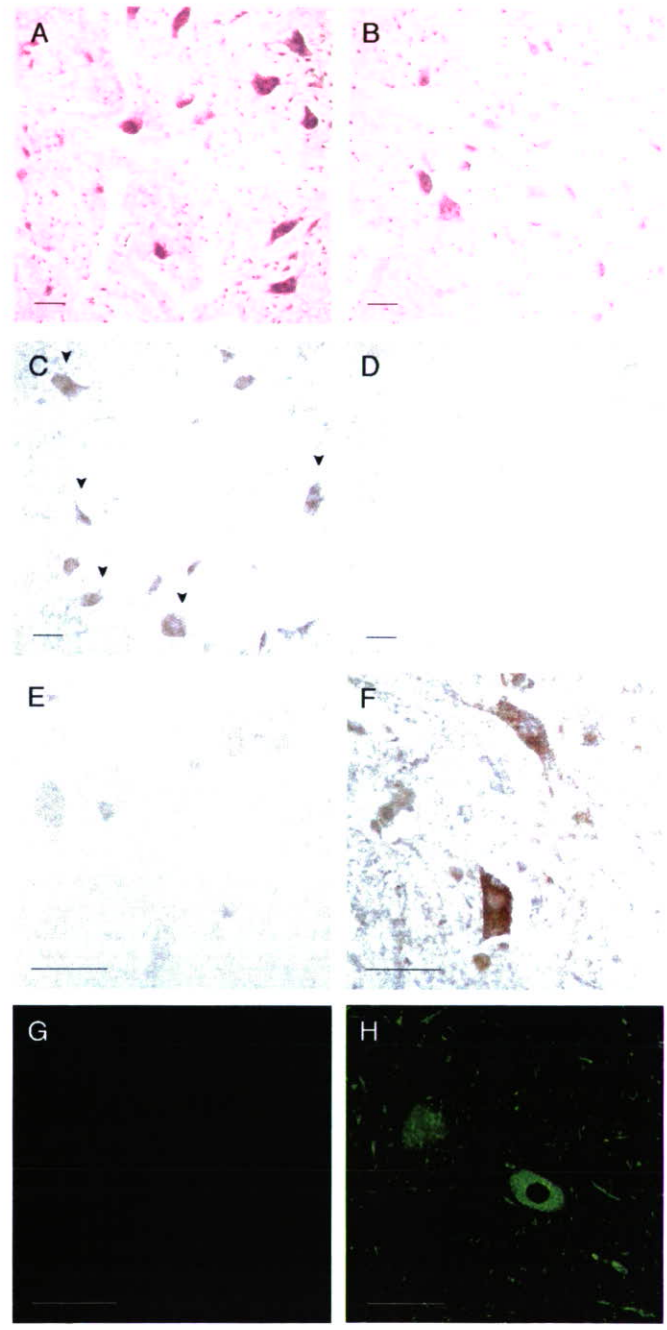

FIGURE 4. Sections of the fifth lumbar anterior horn from G93A transgenic (Tg) rats treated with human recombinant hepatocyte growth factor (hrHGF) **(A, C, E, G)** or vehicle **(B, D, F, H)** for 2 weeks starting at 115 days were stained with hematoxylin and eosin **(A, B)** and antibodies to phosphorylated c-Met **(C, D)**, activated caspase-3 **(E, F)**, and activated caspase-9 **(G, H)**. Scale bar = 50 μm. There were larger numbers of remaining large motor neurons in hrHGF-treated G93A Tg rats (6.7 ± 1.6) **(A)** than in vehicle-treated G93A Tg rats (2.3 ± 0.9) **(B)**. Phosphorylated c-Met staining was more distinct in hrHGF-treated G93A Tg rats **(C)** than in vehicle-treated G93A Tg rats **(D)**. In contrast, activated caspase-3 staining was stronger in vehicle-treated G93A Tg rats **(F)** than in hrHGF-treated G93A Tg rats **(E)**. Activated caspase-9 staining was detectable in vehicle-treated G93A Tg rats **(H)** compared with little reactivity in hrHGF-treated G93A Tg rats **(G)**.